



AMERICAN METEOROLOGICAL SOCIETY

Journal of Climate

EARLY ONLINE RELEASE

This is a preliminary PDF of the author-produced manuscript that has been peer-reviewed and accepted for publication. Since it is being posted so soon after acceptance, it has not yet been copyedited, formatted, or processed by AMS Publications. This preliminary version of the manuscript may be downloaded, distributed, and cited, but please be aware that there will be visual differences and possibly some content differences between this version and the final published version.

The DOI for this manuscript is doi: 10.1175/JCLI-D-15-0475.1

The final published version of this manuscript will replace the preliminary version at the above DOI once it is available.

If you would like to cite this EOR in a separate work, please use the following full citation:

Zhang, W., G. Vecchi, H. Murakami, T. Delworth, A. Wittenberg, A. Rosati, S. Underwood, W. Anderson, L. Harris, R. Gudgel, S. Lin, G. Villarini, and J. Chen, 2015: Improved Simulation of Tropical Cyclone Responses to ENSO in the Western North Pacific in the High-Resolution GFDL HiFLOR Coupled Climate Model. *J. Climate*. doi:10.1175/JCLI-D-15-0475.1, in press.



1 **Improved Simulation of Tropical Cyclone Responses to ENSO in**
2 **the Western North Pacific in the High-Resolution GFDL**
3 **HiFLOR Coupled Climate Model**

4
5 W. Zhang^{1,2}, G. A. Vecchi^{1,2}, H. Murakami^{1,2}, T. Delworth^{1,2}, A.T.
6 Wittenberg¹, A. Rosati¹, S. Underwood⁴, W. Anderson¹, L. Harris¹, R.
7 Gudgel¹, S.-J. Lin¹, G. Villarini³, and J.-H. Chen^{1,2}

8
9 ¹National Oceanic and Atmospheric Administration/Geophysical Fluid
10 Dynamics Laboratory, Princeton, NJ, USA

11 ²Atmospheric and Oceanic Sciences Program, Princeton University,
12 Princeton, NJ, USA

13 ³IIHR-Hydroscience & Engineering, The University of Iowa, Iowa City,
14 Iowa

15 ⁴Engility Corporation, Chantilly, Virginia

16
17 *Corresponding author:

18 Wei Zhang, Ph.D.

19 National Oceanic and Atmospheric Administration/Geophysical Fluid
20 Dynamics Laboratory, Princeton, NJ, USA, 08540

21 Phone: 609-452-5817

22 Email: wei.zhang@noaa.gov

23

24

Abstract

25
26 This study aims to assess whether, and the extent to which, an increase in atmospheric
27 resolution in versions of the Geophysical Fluid Dynamics Laboratory (GFDL)
28 High-Resolution Forecast-oriented Low Ocean Resolution Version of CM2.5 (FLOR)
29 with 50 km and HiFLOR with 25 km improves the simulation of the El Niño Southern
30 Oscillation-tropical cyclone (ENSO-TC) connections in the western North Pacific
31 (WNP). HiFLOR simulates better ENSO-TC connections in the WNP including TC
32 track density, genesis and landfall than FLOR in both long-term control experiments
33 and sea surface temperature (SST)- and sea surface salinity (SSS)-restoring historical
34 runs (1971-2012). Restoring experiments are performed with SSS and SST restored to
35 observational estimates of climatological SSS and interannually-varying monthly SST.
36 In the control experiments of HiFLOR, an improved simulation of the Walker
37 circulation arising from more realistic SST and precipitation is largely responsible for
38 its better performance in simulating ENSO-TC connections in the WNP. In the
39 SST-restoring experiments of HiFLOR, more realistic Walker circulation and steering
40 flow during El Niño/La Niña are responsible for the improved simulation of
41 ENSO-TC connections in the WNP. The improved simulation of ENSO-TC
42 connections with HiFLOR arises from a better representation of SST and better
43 responses of environmental large-scale circulation to SST anomalies associated with
44 El Niño/La Niña. A better representation of ENSO-TC connections in HiFLOR can
45 benefit the seasonal forecasting of TC genesis, track and landfall, improve our

46 understanding of the interannual variation of TC activity, and provide better
47 projection of TC activity under climate change.

48

49 **1. Introduction**

50 Tropical cyclones (TCs) are among the most destructive natural hazards
51 (Emanuel, 2005; Pielke Jr et al., 2008; Peduzzi et al., 2012; Zhang et al., 2009). The
52 scientific community has paid considerable attention to the analysis of their genesis
53 (Chia and Ropelewski, 2002; Gray, 1979; Zehr, 1992; Gray, 1998), track (Riehl and
54 Shafer, 1944; Chan, 1980; Fraedrich and Leslie, 1989; Harr and Elsberry, 1991;
55 Dobos and Elsberry, 1993; Holland and Lander, 1993), landfall (Tuleya et al., 1984;
56 Chan and Liang, 2003; Lyons, 2004) and intensity (Dvorak, 1984; Chan et al., 2001;
57 Emanuel et al., 2004; Wong and Chan, 2004). Advances in the understanding of the
58 physical and dynamical processes of TCs have been achieved with previous studies.

59 The El Niño Southern Oscillation (ENSO) phenomenon plays an important
60 role in modulating the statistics of TC development, genesis and track. ENSO arises
61 from air-sea interactions in the tropical Pacific (Rasmusson and Carpenter, 1982;
62 Philander, 1983; Cane and Zebiak, 1985), and modulates weather and climate not only
63 in the tropics but also the subtropics and extratropics by teleconnections (Wunsch,
64 1991; Lau and Yang, 1996; Lau and Nath, 1996; Alexander et al., 2002). Mounting
65 evidence has supported the influence of ENSO on TC genesis (Chan, 1985; Wu and
66 Lau, 1992; Chan, 2000; Wang and Chan, 2002; Fudeyasu et al., 2006; Wang et al.,

67 2007), intensity (Camargo and Sobel, 2005; Chan, 2008; Zhang et al., 2015a), track
68 (Wang and Chan, 2002; Camargo et al., 2007; Hong et al., 2011; Li and Zhou, 2012),
69 and landfall (Wu et al., 2004; Fudeyasu et al., 2006; Zhang et al., 2012) in the western
70 North Pacific (WNP) based on observations. For example, El Niño (La Niña) favours
71 (suppresses) basin-wide TC activity measured by accumulated cyclone energy in the
72 WNP and enhances TC genesis in the southeastern (northwestern) portion of the WNP
73 (Wang and Chan, 2002; Camargo et al., 2005). More intense typhoons tend to occur
74 during El Niño than La Niña because of the eastward shift in TC genesis and a longer
75 time spent over warmer water and within a moister environment (Wang and Chan,
76 2002; Camargo et al., 2005; Zhang et al., 2015a). In addition, TCs are more likely to
77 make landfall over East Asia during La Niña years because of a westward shift of TC
78 genesis and of the subtropical high (Wu et al., 2004; Zhang et al., 2012). In contrast,
79 there are more recurving TCs during the El Niño than the La Niña phase (e.g., Wang
80 and Chan, 2002; Hong et al., 2011). TC recurvature is a special type of TC track,
81 turning from westward toward the north and eventually to the northeast in the
82 Northern Hemisphere (Riehl and Shafer, 1944; George and Gray, 1977).

83 This connection between TCs and ENSO in the WNP is present not only in the
84 observational records but is also captured by dynamical models (e.g., Wu and Lau,
85 1992; Murakami et al., 2011; Chen and Tam, 2010; Kim et al., 2014; Li and Wang,
86 2014; Vecchi et al., 2014; Krishnamurthy et al., 2015b). Over the decades, models
87 ranging in complexity from atmospheric general circulation models (AGCMs) to

88 coupled general circulation models (CGCMs), have been widely used to simulate the
89 ENSO-TC connections (Wu and Lau, 1992; Camargo and Sobel, 2005; Murakami and
90 Wang, 2010; Murakami et al., 2011; Bell et al., 2014; Wang et al., 2014). The
91 TC-permitting High Resolution Atmospheric Model (HiRAM) has produced
92 promising simulations of inter-annual variability of hurricanes by prescribing the
93 observed sea surface temperature (SST) in the North Atlantic (e.g., Zhao et al., 2009,
94 2010; Chen and Lin, 2011, 2013). CGCMs have also shown encouraging ability to
95 simulate the ENSO-TC connections across the tropics (Kim et al., 2014; Vecchi et al.,
96 2014; Wang et al., 2014; Krishnamurthy et al., 2015b; Murakami et al., 2015). AGCMs
97 have been used for about two decades to simulate the ENSO-TC association in the
98 WNP and have greatly advanced our understanding of the interannual variation of
99 TCs over that region (Wu and Lau, 1992; Vitart and Anderson, 2001; Camargo et al.,
100 2005; Murakami et al., 2011; Li and Wang, 2014; Shaevitz et al., 2014). The 50-km
101 AGCM used by Zhao et al. (2009) has lower skill in simulating the interannual
102 variability of TC genesis frequency over the WNP than over the North Atlantic forced
103 with SST prescribed from the observations. The value of AGCMs forced by historical
104 SSTs to disentangle the role of climate variability on tropical cyclone activity is
105 limited by relatively short integration lengths of these runs, as well as because the
106 observed history of SSTs includes both the impact of radiative forcing and internal
107 variability. In addition, AGCMs do not allow for ocean response to the atmosphere.
108 Therefore, it is relatively difficult to isolate the impacts of such forcing when

109 analysing ENSO-TC connections. In contrast to a number of studies using AGCMs,
110 relatively few studies have focused on the ENSO-TC association in the WNP by using
111 CGCMs (Iizuka and Matsuura, 2008; Bell et al., 2014; Kim et al., 2014; Vecchi et al.,
112 2014; Krishnamurthy et al., 2015b; Murakami et al., 2015).

113 High-resolution CGCMs have shown better skill than lower resolution
114 CCGMs in the simulation of ENSO variability (Shaffrey et al., 2009; Delworth et al.,
115 2012; Dawson et al., 2013; Vecchi et al., 2014; Krishnamurthy et al., 2015b;
116 Murakami et al., 2015). A new high-resolution coupled climate model has been
117 developed at the National Oceanic and Atmospheric Administration
118 (NOAA)-Geophysical Fluid Dynamics Laboratory (GFDL), which is called GFDL
119 Forecast-oriented Low Ocean Resolution Version of CM2.5 (FLOR) (Vecchi et al.,
120 2014; Jia et al., 2015a; Krishnamurthy et al., 2015b; Yang et al., 2015a). FLOR was
121 developed to be part of the North American Multi-Model Ensemble (NMME, Kirtman
122 et al., 2014). FLOR has been used to understand regional seasonal TC activity, and to
123 simulate and predict regional and extreme climate over regions of the world (Vecchi
124 et al., 2014; Msadek et al. 2014; Jia et al., 2015a, 2015b; Krishnamurthy et al., 2015a,
125 2015b; Yang et al., 2015a, 2015b; Zhang et al. 2015b). Although FLOR produces a
126 relatively satisfactory ENSO-TC association in the WNP, the responses of TC density
127 and genesis to ENSO still have relatively large bias in this model (Vecchi et al., 2014;
128 Krishnamurthy et al. 2015b). The regions with positive correlation between Niño3.4
129 and TC track density in the Pacific shift eastward to the eastern Pacific in FLOR and

130 this shift in TC density may arise from stronger El Niño events in FLOR, with a more
131 eastward extension to their convective anomalies resulting in an enhanced negative
132 response in the eastern Pacific and North Atlantic and the eastward extension of the
133 western Pacific positive correlation (Vecchi et al., 2014; Krishnamurthy et al., 2015b;
134 Murakami et al., 2015). Recently, a new high-resolution FLOR (HiFLOR) with 25-km
135 mesh has been developed in GFDL. Initial results indicate that it produces much
136 improved hurricane simulations, especially for the category 4-5 hurricanes (Murakami
137 et al., 2015). The biases in the ENSO amplitude are also reduced in HiFLOR
138 (Murakami et al., 2015). Based on these results, we assess whether and to what extent
139 ENSO-TC connections in the WNP are better captured by HiFLOR. If HiFLOR
140 indeed produces a better simulation of the ENSO-TC connections then this leads us to
141 the question as to how this impacts seasonal forecasting of TC activity and provides
142 us with an opportunity to advance our understanding of the mechanisms underpinning
143 the ENSO-TC linkage from a modeling perspective. Better understanding of
144 ENSO-TC interaction can in turn benefit the simulation and prediction of TCs in the
145 WNP, and produce more reliable projection of TC frequency, genesis, track and
146 landfall under global warming.

147 The remainder of this paper is organized as follows. Section 2 presents data
148 and methodology and Section 3 discusses the analysis results based on observation
149 and simulations with FLOR and HiFLOR. Section 4 presents the discussion and
150 conclusion.

151 **2. Data and Methodology**

152 **2.1 Data**

153 This study uses National Center for Environmental Prediction/National Center
154 for Atmospheric Research (NCEP/NCAR) reanalysis (Kalnay et al., 1996) available
155 from 1948, and Japan Meteorology Agency reanalysis (JRA-55, Kobayashi et al.,
156 2015) data sets starting from 1961 for observed environmental large-scale circulation.
157 Because the results based on two reanalysis datasets are consistent, we only show
158 results from JRA-55. SST data are obtained from the Met Office Hadley Centre with a
159 spatial resolution of $1^{\circ}\times 1^{\circ}$ (Rayner et al., 2003). TC data are from the International
160 Best Track Archive for Climate Stewardship (IBTrACS; Knapp et al., 2010),
161 including latitude, longitude, date and intensity of historical TCs. The $2.5^{\circ}\times 2.5^{\circ}$
162 monthly precipitation data are obtained from Global Precipitation Climatology (GPCP)
163 Project from 1979 to present (Adler et al., 2003).

164 **2.2 Climate models**

165 Models used in this study include state-of-the-art CGCMs: FLOR and
166 HiFLOR. The high-resolution TC-resolving coupled GFDL climate model FLOR was
167 developed to study extreme weather and climate events such as TCs, extratropical
168 cyclones, precipitation extremes and floods (e.g., Vecchi et al., 2014; Jia et al., 2015a,
169 2015b; Yang et al., 2015a, 2015b). The atmosphere and land components are identical
170 to those of the GFDL Climate Model version (CM) 2.5 (Delworth et al., 2012) with a
171 spatial resolution of $50\text{ km}\times 50\text{ km}$. The ocean and sea ice components of FLOR are

172 directly obtained from the CM 2.1 with a spatial resolution of $1^\circ \times 1^\circ$ except that there
173 is refinement of the grid in the deep tropics (from 10°S to 10°N) to approximately $1/3$
174 degree in the meridional direction. The relatively low-resolution ocean and sea ice
175 components in FLOR are designed for a better efficiency of seasonal forecasting with
176 large ensembles.

177 GFDL has developed a higher-resolution version of FLOR (HiFLOR) with a
178 spatial resolution of 25 km based on FLOR (Murakami et al., 2015). HiFLOR was
179 developed by increasing the horizontal resolution of atmosphere and land components
180 while retaining the parameterized physical processes, with the ocean components
181 directly inherited from FLOR except for the length of dynamical integration time
182 steps in the atmosphere. Due to the increasing of the dynamical core atmospheric
183 resolution, the dynamical time-step in HiFLOR is half of that in FLOR. The “physics”
184 time-step (time-step of the convection, cloud and radiation schemes) in HiFLOR is
185 kept the same as FLOR (Murakami et al., 2015). Therefore, the differences between
186 FLOR and HiFLOR lie fundamentally in the horizontal spatial resolution of the
187 atmosphere and land components.

188 **2.3 Experiments**

189 Control experiments were run for 300 years in HiFLOR and 1500 years in
190 FLOR by prescribing radiative forcing representative of 1990. We selected the first
191 300 years from FLOR control experiment to be consistent with HiFLOR and to be
192 compared with 300-year control simulation of HiFLOR. Such experiments are

193 so-called "free run" in which flux adjustments (Magnusson et al. 2013; Vecchi et al.
194 2014) are not applied. It is noted that the control experiments are performed under
195 idealized time-invariant forcing.

196 In addition to the control experiments with FLOR and HiFLOR, restoring
197 experiments over the period 1971-2012 were performed with sea surface salinity
198 (SSS) and SST restored to observational estimates of climatological SSS and
199 interannually-varying monthly SST at time scales of five and ten days (Murakami et
200 al., 2015). The simulated SSS in both models was restored to the World Ocean Atlas
201 2005 (Antonov et al. 2006) and SST was nudged (restored) to the monthly average
202 field obtained from the UK Met Office Hadley Centre SST (HadISST1.1; Rayner et
203 al., 2003). The restoring experiments were conducted with three different initial
204 conditions for both 5-day and 10-day restoring time scales. The difference in TC
205 simulation between 5-day and 10-day restoring time scales was small for both FLOR
206 and HiFLOR (Murakami et al., 2015), so we treat all six members as a single
207 population from each model, thereby yielding six ensemble simulations each for
208 FLOR and HiFLOR. Because both restoring experiments have the same prescribed
209 SST and SSS, these experiments enable the diagnosis of whether and to what extent
210 the differences in the ENSO-TC association between FLOR and HiFLOR arise from
211 the improved performance of the SST simulation.

212 **2.4 Classification of El Niño and La Niña years**

213 The observed TC responses to ENSO are here used as a benchmark for the
214 comparisons between FLOR and HiFLOR. The El Niño and La Niña years are
215 defined based on the Niño3.4 index, which is the SST anomalies averaged over the
216 region (5°S – 5°N and 170°E – 120°W). The SST anomalies are defined as the deviation
217 from the monthly climatology over the 1979–2000 period. The July–October (JASO)
218 months during which the Niño3.4 index is larger/smaller than one standard deviation
219 are designated as El Niño/La Niña, respectively (Kim et al., 2009; Chen and Tam,
220 2010). The La Niña and El Niño years for the period of 1961 to 2013 are listed in
221 Table 1.

222 The strength of El Niño and La Niña events from the control experiments of
223 FLOR and HiFLOR has a larger magnitude than the observations (Table 2). One
224 standard deviation of the anomalous monthly SST is also used as the criterion for
225 identifying El Niño/La Niña years for the FLOR/HiFLOR control experiments, which
226 is consistent with Murakami et al. (2015). In the restoring experiments of FLOR and
227 HiFLOR, we use the same definition of El Niño/La Niña years for the period
228 1971–2012 as in observations because SST was restored to observations. The central
229 Pacific (CP) El Niño is not considered because there are few CP El Niño events in the
230 control experiments of FLOR and HiFLOR. Krishnamurthy et al. (2015b) found that
231 the ENSO amplitude affects the ENSO-TC connections; therefore, if we select El
232 Niño/La Niña years from the control experiments of FLOR and HiFLOR using the
233 magnitudes of SST anomalies changing from 0.6°C to 1.4°C at an interval of 0.1°C ,

234 the TC responses to ENSO are still consistent with those using one standard deviation
235 of Niño3.4. In general, the strength of responses of WNP TC to ENSO is indeed
236 stronger for stronger ENSO events.

237 **2.5 Landfall regions**

238 Following previous studies (Wu et al., 2004; Zhang et al., 2012), the East
239 Asian coast is divided into four subregions: Japan and Korea, the Philippines, the
240 Indochina and Malay Peninsula (ICMP), and China. The landfall frequencies are
241 calculated for these four subregions, as well as for East Asia as a whole. Although the
242 Philippines are geographically not part of East Asia, we consider them as one of the
243 subregions since the Philippines are often at severe threat of landfalling tropical
244 systems (Wu et al., 2004; Chan and Xu, 2009; Zhang et al., 2012). In general, TCs are
245 more likely to make landfall over East Asia during La Niña than El Niño phases.

246 **3. Results**

247 This section discusses the analysis of TC activity (e.g., density, genesis and
248 landfall) during El Niño and La Niña phases and examines the ENSO-TC association
249 and underlying mechanisms. This is accomplished based on the control experiments
250 and SSS- and SST-restoring ensemble experiments with both FLOR and HiFLOR and
251 observations.

252 **3.1 Results from Control Experiments**

253 TC density climatology in the 300-year control experiments of HiFLOR,
254 FLOR and observations is shown in Figure 1. TC track/genesis density is obtained by

255 binning the TC tracks/geneses in the WNP in 5×5 degree grid boxes without
256 smoothing. The detailed tracking processes are provided in the Appendix part of this
257 paper. Although the spatial patterns of the TC density climatology in the control
258 experiments of HiFLOR and FLOR are similar, the TC density climatology in
259 HiFLOR is larger than that in FLOR (Figure 1). In contrast to the observations, the
260 centers of TC track density in HiFLOR and FLOR are located eastward (Figure 1) and
261 such spatial characteristics have also been reported in previous studies (Vecchi et al.,
262 2014; Murakami et al., 2015). Similar to the TC track density climatology, the
263 climatology of TC genesis density in the control experiments of HiFLOR and FLOR
264 is located eastward of that in observations (Figure 2). However, the TC genesis
265 density pattern in HiFLOR is closer than that in FLOR to the observations, especially
266 from 120°E to 150°E (Figure 2). The differences in TC genesis and density
267 climatology between HiFLOR and FLOR (HiFLOR minus FLOR) are characterized
268 by a dipole pattern in the WNP, i.e., positive anomalies in the eastern part of the WNP
269 and negative anoamlies in the western part of the WNP (Figure 1S). The seasonal
270 cycle of WNP TC frequency in HiFLOR, FLOR and observations is consistent with
271 the above discussion on TC genesis (Supplemental Figure 2S). HiFLOR simulates
272 TCs more than observations in the WNP for each month and more than FLOR from
273 April to September (Supplemental Figure 2S), similar to what presented by Murakami
274 et al. (2015). However, HiFLOR produces a more faithful representation of the
275 phasing of seasonal cycle of TC frequency in the WNP than FLOR, with the peak in

276 FLOR occurring a month or so after the August peak observed and in HiFLOR
277 (Supplemental Figure 2S). The improvements in the seasonal variation of TC
278 frequency are consistent with previous studies reporting that an increase in horizontal
279 resolution of a climate model results in better seasonal variation of TC frequency in a
280 coupled climate model (Murakami and Sugi, 2010). The simulated mean frequency of
281 TC landfall over East Asia and its subregions in the control experiment of HiFLOR is
282 better than that in FLOR (Supplemental Figure 3S). A better simulation of TC
283 climatology can play some role in improving the simulated responses of TCs to
284 ENSO.

285 Distinct differences in TC track density anomalies are found between El Niño
286 and La Niña conditions in the 300-year control experiments with HiFLOR (Figure 3a
287 and 3b). During the El Niño phase of HiFLOR control simulation, positive (negative)
288 TC density anomalies are identified in the eastern (western) WNP. During the La Niña
289 phase, the spatial pattern of TC density anomalies is largely the opposite of what
290 discussed for the El Niño phase although positive anomalies are relatively weak in the
291 Philippine Sea and the South China Sea (Figure 3a and 3b). In the El Niño phase of
292 FLOR control simulation, the positive TC density anomalies are stronger and shifted
293 more eastward toward the central Pacific than HiFLOR. In the La Niña phase of the
294 control simulations with FLOR, the negative TC density anomalies shift more
295 eastward and prevail in the entire WNP. Such TC density patterns during the ENSO

296 phases with FLOR or CM2.5 have been identified in previous studies (Kim et al.,
297 2014; Vecchi et al., 2014; Krishnamurthy et al., 2015b; Murakami et al., 2015).

298 TC density anomalies in HiFLOR are more consistent with observations than
299 FLOR during both El Niño and La Niña phases. In the El Niño phase, the centre of
300 positive TC density anomalies are shifted more westward in HiFLOR than in FLOR
301 (Figure 3) with the spatial pattern of negative/positive TC density anomalies in
302 HiFLOR closer to the observations, although some eastward bias still exists. During
303 El Niño, there are positive TC density anomalies around the Philippines in FLOR
304 while there are negative TC density anomalies in HiFLOR and the observations in this
305 region. In the La Niña phase, HiFLOR produces a better simulation of TC track
306 density than FLOR, in that both HiFLOR and observations show positive TC density
307 anomalies in the South China Sea and the East Asian coast in contrast to basin-wide
308 negative TC density anomalies in FLOR.

309 The regressions of TC density onto Niño3.4 is shown to further substantiate
310 the previous discussion (Figure 4). The regressions of TC track density anomalies
311 onto the Niño3.4 index with HiFLOR resemble those from observations while the
312 positive anomalies from FLOR have a much higher magnitude (Figure 4). This
313 indicates that the responses of TC density to ENSO in FLOR are much stronger than
314 the observations and HiFLOR. Although the positive anomalies of TC track density in
315 HiFLOR control experiments are shifted slightly eastward when compared to the
316 observations (though less so than in FLOR), the magnitude of anomalous TC track

317 density is in good agreement (Figure 4). Compared with the observations, regression
318 analysis discussed above suggests that the responses of TC density to a unit of
319 Niño3.4 (i.e., 1°C) are stronger in FLOR than either HiFLOR or observations,
320 especially in the eastern part of the WNP. Different sample sizes (time period) in the
321 control experiments and observations may bias the above results. We calculate the
322 regression of TC track density onto Niño3.4 index in each 53-year sub-period (the
323 same as the time period (1961-2013) of observations) in the control experiments of
324 HiFLOR and FLOR (not shown). It appears that the regression of TC density onto
325 Niño3.4 over the entire 300 years is consistent with those over every 53-year
326 sub-periods in the control experiments of HiFLOR and FLOR.

327 Consistent with the above discussion, HiFLOR also produces TC genesis
328 anomalies that are in closer agreement with the observations than FLOR in ENSO
329 phases (Figure 5). Specifically, TC genesis anomalies in FLOR are located
330 substantially further eastward than in the observations during the El Niño phase. In
331 contrast, TC genesis in HiFLOR is located more westward than in FLOR, more
332 similar to observations in the El Niño phase (Figure 5). During the La Niña phase,
333 FLOR does not reproduce the observed positive anomalies west of 140°E, whereas
334 HiFLOR shows the positive TC genesis anomalies, especially over the area from
335 120°E to 140°E (Figure 5).

336 Previous studies have reported that landfalling TCs over East Asia are more
337 likely to occur in La Niña years than El Niño years because of a westward shift in the
338 subtropical high during la Niña years which subsequently produces an increase in TC
339 landfall in the WNP (Wang and Chan, 2002; Wu et al., 2004; Zhang et al., 2012).
340 Figure 6 lists the correlation coefficients between the frequency of TCs making
341 landfall over East Asia and four subregions and Niño3.4 in the control simulation of
342 FLOR and HiFLOR and observations (1961-2013). The correlation in HiFLOR more
343 closely resembles what obtained from the observation than in FLOR except for TC
344 landfall over Japan and Korea (Figure 6). There is a much stronger positive
345 correlation between landfall over Japan and Korea during La Niña in HiFLOR than
346 observations (Figure 6). In addition, the correlation between TC landfall over China
347 and Niño3.4 in FLOR is positive while it is negative in the observations and HiFLOR
348 (Figure 6). HiFLOR therefore makes a substantial improvement in simulating the
349 responses of TC landfall over China to ENSO. It is of great significance because
350 China is a heavily populated country and has the longest coastline in East Asia.
351 Moreover, the association between the frequency of TC landfall over East Asia and
352 subregions and Niño3.4 is largely better simulated in HiFLOR than in FLOR. The
353 improved connection between TC track density and ENSO in HiFLOR is thus
354 reflected in a better connection between TC landfall and ENSO.

355 **3.2 Mechanisms from control experiments**

356 ENSO alters remote large-scale circulation by teleconnections (Lau and Nath,
357 1996; Alexander et al., 2002). The modulation of the Walker circulation by ENSO
358 strongly shapes the ENSO-TC connections in the WNP in FLOR and HiFLOR. The
359 SST, precipitation, the Walker circulation and steering flow during El Niño and La
360 Niña phases in HiFLOR, FLOR and observations are discussed to identify the
361 underlying mechanisms.

362 The standard deviation of Niño3.4 in HiFLOR is smaller than those in FLOR
363 but still larger than in the observations (Table 2). The SST anomaly patterns during El
364 Niño and La Niña phases from HiFLOR, FLOR and the observations are shown in
365 Figure 7; SST anomalies in FLOR are stronger than those in HiFLOR and in the
366 observations for both El Niño and La Niña phases, especially in the ENSO regions
367 (Figure 7a, c, and e). A larger magnitude of Niño3.4 in FLOR may be responsible for
368 the stronger responses of TC density to ENSO as shown in Figure 2 (Krishnamurthy
369 et al., 2015b; Murakami et al., 2015).

370 Precipitation is closely linked to SST anomaly patterns. Precipitation is
371 associated with deep convection in the atmosphere, which alters local and remote
372 circulation (Trenberth et al., 2002; Chiang and Lintner, 2005). During El Niño years,
373 the FLOR precipitation anomalies are stronger than those in HiFLOR and in the
374 observations in the tropical central Pacific, indicating the responses of precipitation to
375 SST anomalies in HiFLOR bear more resemblance than FLOR to those in the
376 observations (Figure 8). During La Niña years, the major differences in precipitation

377 anomalies between HiFLOR and FLOR are located in the southeastern WNP
378 (depicted by the rectangles in Figure 8d and 8f). The precipitation anomalies in the
379 marked regions of Figure 8 are also reflected in the Walker circulation (Figure 9).

380 TC activity in the WNP is largely modulated by dynamic factors associated
381 with changes in large-scale circulation rather than local thermo-dynamic changes
382 connected to local SST (Chan, 2000; Wang and Chan, 2002; Chan and Liu, 2004; Fu
383 et al., 2011). Changes in the Walker Circulation are exhibited in the vertical profiles of
384 zonal wind (averaged over 5°N to 20°N) and $-50 \cdot \omega$ (unit: pa/s) (Figure 9). During El
385 Niño years, the anomalous updraft in the tropical central Pacific in FLOR is much
386 stronger than those in HiFLOR and observations (i.e., JRA-55 reanalysis) (Figure 9),
387 suggesting stronger deep convection over that region in FLOR. Such results
388 corroborate the analysis of TC density and genesis anomalies in HiFLOR, FLOR and
389 the observations (Figures 3 and 4).

390 During La Niña years, the updraft anomalies in the control simulation of
391 FLOR are still greater than in HiFLOR and the anomalous downdraft in FLOR is also
392 stronger than in HiFLOR in the WNP (Figure 9), resulting in strong suppression of
393 WNP TC activity in FLOR. In addition, the Walker circulation in HiFLOR is more
394 realistic than that in FLOR, particularly the anomalous ascent in the WNP and the
395 anomalous subsidence in the tropical eastern and central Pacific (Figure 9d). The
396 excessive anomalous Walker circulation appears responsible for the heightened

397 negative TC density and genesis anomalies in the WNP during La Niña years in the
398 FLOR control experiment.

399 Figure 10 illustrates the differences in the steering flow (850 hPa - 200 hPa
400 mass-weighted mean) between HiFLOR and FLOR in the control experiments during
401 El Niño and La Niña phases. HiFLOR produces a stronger easterly steering flow than
402 FLOR in both El Niño and La Niña phases, indicating that WNP TCs are more likely
403 to move westward in HiFLOR given the same genesis locations (Figure 10). The
404 effects of steering flow appear to be highly distinct in the La Niña phase in the control
405 experiments of HiFLOR and FLOR because TC density in HiFLOR is much higher
406 than that in FLOR (Figures 3 and 9). Although higher TC genesis in the Philippine
407 Sea may play some role in shaping the differences in TC density between HiFLOR
408 and FLOR, the steering flow should act as a key factor to produce different TC
409 density patterns during La Niña phase. Previous studies have shown that the beta drift
410 due to Coriolis force changes related to TC size also influence TC tracks (Wu and
411 Wang, 2000, 2001). As shown in Murakami et al. (2015), TC sizes in FLOR and
412 HiFLOR are very close to one another, indicating that beta drift is not an important
413 factor in causing the differences between FLOR and HiFLOR.

414 **3.3 SST-restoring experiments**

415 The previous discussion has shown that the responses of TC density, genesis
416 and landfall to ENSO are greatly improved in HiFLOR than FLOR in the control
417 experiments. Since the ENSO SST anomalies in FLOR are much stronger than those

418 in HiFLOR and in the observations, it is useful to assess whether the ENSO-TC
419 improvements are caused by a better representation of SST in HiFLOR. We do so by
420 exploring whether, and the extent to which the improvements between HiFLOR and
421 FLOR in simulated ENSO-TC relationship still hold in the additional SST and SSS
422 restoring ensemble experiments which control for differences in SST simulation in the
423 coupled models.

424 The climatology of TC track density in the SSS- and SST-nudging
425 experiments of HiFLOR is larger than that in FLOR in period 1971–2012 and both
426 have similar spatial patterns (Figure 11). The high centers of TC track density
427 climatology in HiFLOR and FLOR reside eastward of those in the observations in
428 1971–2012 (Figure 11). The high centers of TC genesis density climatology in
429 HiFLOR and FLOR are also located eastward of that in the observations (Figure 12).
430 However, the genesis density climatology in HiFLOR is located less eastward than
431 that in FLOR, indicating a stronger resemblance to the observations than FLOR
432 (Figure 12). The seasonal variation of WNP TC frequency in HiFLOR more closely
433 resembles the observations than FLOR, although there is a higher TC frequency in
434 HiFLOR for each month (Supplementary Figure 3S). The climatology of TC landfall
435 frequency over the Philippines, ICMP, China and East Asia in the SSS- and SST-
436 restoring experiment of HiFLOR appears to be close to or better than those in FLOR,
437 while FLOR outperforms HiFLOR for TC landfall over Japan and Korea (Figure 4S).

438 In the El Niño phase, TC track density anomalies in the SST-restoring
439 experiments with HiFLOR are consistent with those in the observations, while those
440 with FLOR differ considerably from observations (Figure 13). Both TC track density
441 anomalies in the SST-restoring experiments with HiFLOR and the observations
442 feature a dipole mode in the WNP (Figure 13). In contrast, the TC track density
443 anomalies in the SST-restoring experiments with FLOR have strong positive
444 anomalies in the eastern WNP (Figure 13). During El Niño years, there are negative
445 TC density anomalies near the East Asian coast in both observations and the
446 SST-restoring experiments with HiFLOR, while negative anomalies are not observed
447 in FLOR. Instead, positive TC density anomalies are observed in the northern
448 Philippines (Figure 13c). During La Niña years, positive TC track density anomalies
449 prevail along the East Asian coast, while there are strong negative TC track density
450 anomalies in the WNP in the observations (Figure 13f). Such TC density anomalies
451 suggest more TCs making landfall over East Asia during the La Niña phase (Wu et al.,
452 2005; Zhang et al., 2012). The SST-restoring experiments with HiFLOR largely
453 reproduce the TC track density anomalies in the observations during La Niña (Fig.
454 13b). The TC track density anomalies in FLOR (Fig. 13d), however, are quite
455 different from those in the observations because there are negative TC density
456 anomalies almost everywhere in the WNP. Based on the SST-restoring experiments
457 with FLOR, there are less TC landfalls over East Asia during La Niña years, which is
458 the opposite to what found in the observations. Therefore, our finding that HiFLOR

459 produces better responses of TC to ENSO than FLOR based on 300-year control
460 experiments also holds for the SST-restoring ensemble experiments.

461 The differences in TC genesis locations between HiFLOR and FLOR are
462 mainly located west of 150°E (Fig. 14). During the El Niño phase, negative TC
463 genesis anomalies are stronger in FLOR than HiFLOR west of 150°E. TC density
464 anomalies in FLOR are, however, higher than in HiFLOR in the vicinity of the East
465 Asian coast during the El Niño phase. During the La Niña phase, positive TC genesis
466 anomalies are stronger in HiFLOR than in FLOR west of 150°E, consistent with TC
467 density patterns (Figures 13 and 14). However, TC genesis cannot fully explain the
468 spatial patterns of TC density, especially during the El Niño phase. Therefore, the
469 steering flow between HiFLOR and FLOR may be responsible for the differences in
470 TC density.

471 The correlations between TC landfall and Niño3.4 based on FLOR, HiFLOR
472 and observations are listed in Table 3. Such correlations are consistent with those in
473 the control experiments (Figure 6). HiFLOR reproduces the negative correlation
474 between the frequencies of TCs making landfall over East Asia and the subregions
475 and Niño3.4 in the observational records, though the correlation coefficients have a
476 larger magnitude (Table 3). In contrast, FLOR produces positive correlation
477 coefficients between Niño3.4 and the frequencies of TCs making landfall over China
478 and East Asia, with the wrong sign compared with those based on observations (Table
479 3). Meanwhile, the correlation coefficients between Niño3.4 and the frequencies of

480 TCs making landfall over Japan and Korea, the Philippines, and ICMP in FLOR are
481 similar to those in observations.

482 **3.4 Mechanisms from SST-restoring experiments**

483 Since SST in the restoring experiments with HiFLOR and FLOR are restored
484 to the observations, only the precipitation, the Walker circulation and steering flow
485 during El Niño and La Niña phases are discussed here.

486 During the El Niño phase, the precipitation anomalies located in the WNP in
487 HiFLOR and FLOR restoring experiments are largely weaker than those in the
488 observations (Figure 15). The precipitation anomalies in HiFLOR and FLOR are
489 similar to one another in the WNP, suggesting similar strengthen of deep convection
490 in HiFLOR and FLOR (Figure 15). During the La Niña phase, the precipitation
491 anomalies in the WNP in FLOR and HiFLOR are similar to the observations (Figure
492 15).

493 This is in contrast with the precipitation anomalies in HiFLOR and FLOR for
494 the control experiments, where FLOR produces stronger positive anomalies in
495 precipitation than HiFLOR. The SST-restoring experiments of FLOR and HiFLOR
496 have similar observationally-based SST patterns, but FLOR overestimates ENSO
497 amplitude in its control experiment. The weaker responses of precipitation to El
498 Niño/La Niña in the restoring experiments of FLOR may arise from the weaker SST
499 anomalies compared with the control experiments of FLOR. This also indicates the
500 important role SST plays in shaping the deep convection.

501 Figure 16 shows the vertical profile of wind vector, i.e., zonal wind (averaged
502 over 5°N - 20°N) and $-50 \cdot \omega$ (unit: pa/s) during El Niño and La Niña phases based on
503 the SST-restoring experiments with HiFLOR, FLOR and the observations. The
504 differences in the Walker circulation between FLOR and HiFLOR are mainly located
505 in 110°E - 150°E (Figure 16). In the El Niño phase, the updraft anomalies in FLOR is
506 stronger than HiFLOR in 110°E - 150°E. In the La Niña phase, the downdraft
507 anomalies in FLOR is also stronger than HiFLOR in 110°E - 150°E (Figure 16). This
508 is consistent with the differences in TC genesis anomalies between HiFLOR and
509 FLOR during El Niño and La Niña years in 110°E - 150°E (Figure 14)

510 Figure 13 also shows that TCs in FLOR tend to move towards the East Asian
511 coast in the El Niño phase while they tend to stay in the ocean during the La Niña
512 phase. In addition to the spatial patterns of TC genesis, the differences in steering
513 flow between HiFLOR and FLOR (HiFLOR - FLOR) SST-nudging experiments are
514 also analysed during both El Niño and La Niña phases (Figure 17). Steering flow (850
515 - 200 hPa) is more favourable for TCs to move eastward in HiFLOR than FLOR
516 during the El Niño phase (Figure 17). Meanwhile, steering flow is more conducive to
517 westward-moving TC track from 10°N to 20°N in HiFLOR than FLOR during the La
518 Niña phase (Figure 17). This is partly responsible for strong negative TC track density
519 anomalies in the WNP in FLOR and strong positive TC track density anomalies along
520 the East Asian coast in HiFLOR during the La Niña phase. Such characteristic TC
521 density anomalies can be attributed to the steering flow patterns in FLOR and

522 HiFLOR (Figure 17). Therefore, the responses of the Walker Circulation (averaged
523 over 5°N - 20°N) and steering flow to ENSO in HiFLOR are better simulated than
524 FLOR in the restoring ensemble experiments. Such responses contribute, in addition
525 to the improved simulation of ENSO, to the improved simulation of TC density and
526 genesis in HiFLOR.

527 **4. Discussion and conclusions**

528 ENSO-TC connections in the WNP have attracted tremendous attention over
529 the decades, with analyses based on both observations and dynamic models. Over
530 time, AGCMs and CGCMs have reported large improvements in the simulation of
531 ENSO-TC connections. However, the performance of such simulations is not yet
532 satisfactory because of remaining model biases and gaps in our understanding of
533 ENSO-TC connections.

534 Although the GFDL CM 2.5 has shown encouraging results for the responses
535 of TC activity to ENSO, a larger eastward shift and higher magnitude in anomalous
536 TC density in the WNP were found during El Niño/La Niña phases compared to the
537 observations (Kim et al., 2014). FLOR inherits this ENSO-TC association in the WNP
538 from CM2.5 as reported in Vecchi et al. (2014). Recently, GFDL has developed the
539 high-resolution FLOR (HiFLOR) with a spatial horizontal resolution of 25 km, which
540 performs much better than FLOR in the simulation of global category-4 and 5 TCs,
541 especially in the North Atlantic (Murakami et al, 2015). This study aims to assess
542 whether and by what mechanisms HiFLOR improves the simulation of ENSO-TC

543 connections in the WNP by using long-term control simulations and restoring
544 ensemble experiments. Our research findings are summarized as follows.

545 1. HiFLOOR simulates better ENSO-TC connections in the WNP including the TC
546 track density, genesis and landfall than FLOR in both long-term control
547 experiments and SST-restoring historical runs (1971–2012).

548 2. In the control experiments of HiFLOOR, an improved simulation of the Walker
549 circulation related to SST and deep convection is largely responsible for its
550 better performance in simulating ENSO-TC connections in the WNP. In the
551 SST-restoring experiments of HiFLOOR, more realistic Walker circulation and
552 steering flow with HiFLOOR during El Niño/La Niña are responsible for the
553 better simulation of TC activity in the WNP.

554 3. An improved simulation of ENSO-TC connections with HiFLOOR arises from a
555 better representation of SST and better responses of environmental large-scale
556 circulation to SST anomalies associated with El Niño/La Niña.

557 Fundamentally, HiFLOOR differs from FLOR because a higher spatial
558 resolution of atmospheric and land components. The enhanced resolution of the
559 atmospheric component in HiFLOOR relative to FLOR results in coupled feedback that
560 drives an improved ENSO SST simulation; the SST in turn drives better atmospheric
561 responses in HiFLOOR (Murakami et al., 2015). This partly explains the better
562 performance of HiFLOOR in simulating ENSO-TC connections in the WNP. However,
563 as demonstrated in the SST-restored experiments, even with the very similar SSTs

564 HiFLOR outperforms FLOR in WNP TCs. Using CGCM with a horizontal resolution
565 of 60-km, the simulated TC genesis is shifted more eastward during La Niña years in
566 contrast to the observations (Iizuka and Matsuura, 2008). Bell et al. (2014) showed
567 that both HiGAM and HiGEM produce encouraging simulations of global ENSO-TC
568 connections. However, large negative (positive) TC track density anomalies are
569 simulated in the western WNP during El Niño/La Niña phases (Bell et al., 2014). This
570 may arise from the different months selected for TC density analysis because the
571 current study analysed TC from July to October while Bell et al. (2014) examined
572 TCs from May to November or from model biases. The current study has shown that
573 HiFLOR performed better than FLOR in simulating ENSO-TC connections in terms
574 of genesis and track and landfall in the WNP. HiFLOR produces simulations
575 comparable to or slightly better than other models and the better simulation with
576 HiFLOR is largely attributed to the more realistic representation of SST and the
577 improved large-scale circulation responses to El Niño/La Niña associated with SST
578 anomalies.

579 Although this study has shown encouraging results for ENSO-TC connections
580 based on state-of-the-art HiFLOR and FLOR, we still need further improvements in
581 the simulation of total TC genesis in the WNP. This is particularly true for the areas
582 with strong TC density anomalies around the East Asian coast and the Philippine Sea
583 in HiFLOR. A better representation of ENSO-TC connections may benefit the
584 seasonal forecasting of TC genesis, track and landfall, improve our understanding of

585 the interannual variation of TC activity and provide better projection of TC activity
586 under climate change. Such analysis will be conducted in our future studies. Because
587 an improved simulation of ENSO-TC connections in the WNP is also observed in
588 SST-restoring experiments, it is thus of great interest to examine whether or not
589 HiFLOR can outperform FLOR in seasonal forecasting of WNP TC activity.

590

591 **Acknowledgement**

592 The authors thank the editor and three anonymous reviewers for insightful comments
593 and suggestions. The authors are grateful to Lakshmi Krishnamurti and Liping Zhang
594 for their valuable comments on an earlier version of this paper. The authors thank
595 Fanrong Zeng for helpful assistance in experiments. This material is based in part
596 upon work supported by the National Science Foundation under Grants AGS-1262091
597 and AGS-1262099.

598

Appendix

599 **Tracking algorithm**

600 The tracker is developed by Harris et al. (in preparation) to track TCs from 6-hour
601 climate simulations. This tracker was also employed in Zhang et al. (2015b) and
602 Murakami et al. (2015). The tracking processes are based on key variables such as
603 temperature, sea level pressure (SLP) and 10-m wind. The tracking procedures are
604 described as follows.

605 (1) Local minima of the smoothed SLP field are found. The location of the center
606 is properly adjusted by fitting a biquadratic function to the SLP and locating
607 the center at the minimum.

608 (2) Closed contours in an interval of 2 hPa (dp) around every single SLP low
609 center. The Nth contour is marked as the contiguous region surrounding a low
610 central pressure P with pressures lower than $dp \times N + P$, as detected by a
611 “flood fill” algorithm. It is noted that the contours are not required to be
612 circular and a maximum radius of 3,000 km will be searched from each
613 candidate low center.

614 (3) If the algorithm detects contours that are close enough, the low is counted in
615 as a TC center. By this way, the tracker attempts to find all closed contours in
616 the vicinity of the low center within a certain distance from the low center and
617 without entering contours belonging to another low. The maximum 10-m wind
618 inside the set of closed contours is taken as the maximum wind speed at that
619 time for the storm.

620 (4) Warm cores are detected via similar processes: closed 1°C contours for FLOR
621 are found surrounding the maximum temperature anomaly (t_a) within a TC's
622 identified contours, no more than 1 degree from the low center. This contour
623 must have a radius smaller than 3 degrees in distance. If there is not such a
624 core, it should not be marked as a warm-core low center, though the center is
625 not rejected.

626 (5) TC centers are combined into a track by taking a low center at time $T - dt$,
627 extrapolating its motion forward dt , and then seeking storms within 750 km. It
628 is noted that a deeper low center has higher priority of tracking.

- 629 (6) The following criteria are required to pick up the final TCs.
- 630 a. At least 72 hours of total detection lifetime (not necessarily
- 631 consecutive).
- 632 b. At least 48 cumulative (not necessarily consecutive) hours with a warm
- 633 core.
- 634 c. At least 36 consecutive hours of a warm core with winds greater than
- 635 17.5 ms^{-1} .
- 636 d. TC genesis should be confined equatorward of 40°N .
- 637
- 638

639 **References**

- 640 Adler, R. F., G. J. Huffman, A. Chang, R. Ferraro, P.-P. Xie, J. Janowiak, B. Rudolf, U.
- 641 Schneider, S. Curtis, D. Bolvin, A. Gruber, J. Susskind, P. Arkin, and E. Nelkin,
- 642 2003: The Version-2 Global Precipitation Climatology Project (GPCP) Monthly
- 643 Precipitation Analysis (1979–Present). *Journal of Hydrometeorology*, 4,
- 644 1147-1167.
- 645 Alexander, M. A., I. Blade, M. Newman, J. R. Lanzante, N.-C. Lau, and J. D. Scott,
- 646 2002: The Atmospheric Bridge: The Influence of ENSO Teleconnections on
- 647 Air-Sea Interaction over the Global Oceans. *Journal of Climate*, 15, 2205-2231.
- 648 Antonov, J. I., R. A. Locarnini, T. P. Boyer, A. V. Mishonov, and H. E. Garcia, 2006:
- 649 Salinity. Vol. 2, *World Ocean Atlas 2005*, NOAA Atlas NESDIS 62, 182 pp.
- 650 Bell, R., K. Hodges, P. L. Vidale, J. Strachan, and M. Roberts, 2014: Simulation of the
- 651 Global ENSO–Tropical Cyclone Teleconnection by a High-Resolution Coupled
- 652 General Circulation Model. *Journal of Climate*, 27, 6404-6422.
- 653 Camargo, S. J. and A. H. Sobel, 2005: Western North Pacific tropical cyclone
- 654 intensity and ENSO. *Journal of Climate*, 18, 2996-3006.
- 655 Camargo, S. J., A. G. Barnston, and S. E. Zebiak, 2005: A statistical assessment of
- 656 tropical cyclone activity in atmospheric general circulation models. *Tellus A*, 57,
- 657 589-604.
- 658 Camargo, S. J., A. W. Robertson, S. J. Gaffney, P. Smyth, and M. Ghil, 2007: Cluster
- 659 analysis of typhoon tracks. Part II: Large-scale circulation and ENSO. *Journal of*
- 660 *Climate*, 20, 3654-3676.
- 661 Cane, M. A. and S. E. Zebiak, 1985: A theory for El Niño and the Southern
- 662 Oscillation. *Science*, 228, 1085-1087.

663 Chan, J. C. L., 1980: Use of Upper and Lower Tropospheric Data for Tropical
664 Cyclone Track Forecasting. *Bulletin of the American Meteorological Society*, 61,
665 1124-1124.

666 Chan, J. C. L., 1985: Tropical Cyclone Activity in the Northwest Pacific in Relation to
667 the El Niño and Southern Oscillation Phenomenon. *Monthly Weather Review*, 113,
668 599-606.

669 Chan, J. C. L., 2000: Tropical cyclone activity over the western North Pacific
670 associated with El Niño and La Niña events. *Journal of Climate*, 13, 2960-2972.

671 Chan, J. C., 2008: Decadal variations of intense typhoon occurrence in the western
672 North Pacific. *Proceedings of the Royal Society A: Mathematical, Physical and
673 Engineering Science*, 464, 249-272.

674 Chan, J. C. L. and X. D. Liang, 2003: Convective asymmetries associated with
675 tropical cyclone landfall. Part I: f-plane simulations. *Journal of the Atmospheric
676 Sciences*, 60, 1560-1576.

677 Chan, J. C. L. and K. S. Liu, 2004: Global Warming and Western North Pacific
678 Typhoon Activity from an Observational Perspective. *Journal of Climate*, 17,
679 4590-4602.

680 Chan, J. C. L. and M. Xu, 2009: Interannual and inter-decadal variations of
681 landfalling tropical cyclones in East Asia. Part I: time series analysis. *International
682 Journal of Climatology*, 29, 1285-1293.

683 Chan, J. C. L., Y. H. Duan, and L. K. Shay, 2001: Tropical cyclone intensity change
684 from a simple ocean-atmosphere coupled model. *Journal of the Atmospheric
685 Sciences*, 58, 154-172.

686 Chen, G. and C.-Y. Tam, 2010: Different impacts of two kinds of Pacific Ocean
687 warming on tropical cyclone frequency over the western North Pacific. *Geophys.
688 Res. Lett.*, 37, L01803.

689 Chen, J.-H. and S.-J. Lin, 2011: The remarkable predictability of interannual
690 variability of Atlantic hurricanes during the past decade. *Geophys. Res. Lett.*,
691 38, L11804

692 Chen, J.-H. and S.-J. Lin, 2013: Seasonal Predictions of Tropical Cyclones Using a
693 25-km-Resolution General Circulation Model. *Journal of Climate*, 26, 380-398.

694 Chia, H. H. and C. Ropelewski, 2002: The interannual variability in the genesis
695 location of tropical cyclones in the northwest Pacific. *Journal of Climate*, 15,
696 2934-2944.

697 Chiang, J. C. H. and B. R. Lintner, 2005: Mechanisms of Remote Tropical Surface
698 Warming during El Niño. *Journal of Climate*, 18, 4130-4149.

699 Dawson, A., A. J. Matthews, D. P. Stevens, M. J. Roberts, and P. L. Vidale, 2013:
700 Importance of oceanic resolution and mean state on the extra-tropical response to
701 El Niño in a matrix of coupled models. *Climate dynamics*, 41, 1439-1452.

702 Delworth, T. L., A. Rosati, W. Anderson, A. J. Adcroft, V. Balaji, R. Benson, K. Dixon,
703 S. M. Griffies, H.-C. Lee, R. C. Pacanowski, G. A. Vecchi, A. T. Wittenberg, F.
704 Zeng, and R. Zhang, 2012: Simulated Climate and Climate Change in the GFDL

705 CM2.5 High-Resolution Coupled Climate Model. *Journal of Climate*, 25,
706 2755-2781.

707 Dobos, P. H. and R. L. Elsberry, 1993: Forecasting Tropical Cyclone Recurvature .1.
708 Evaluation of Existing Methods. *Monthly Weather Review*, 121, 1273-1278.

709 Dvorak, V. F., 1984: Tropical cyclone intensity analysis using satellite data. US
710 Department of Commerce, National Oceanic and Atmospheric Administration,
711 National Environmental Satellite, Data, and Information Service.

712 Emanuel, K., 2005: *Divine Wind-The History and Science of Hurricanes*. Divine
713 Wind-The History and Science of Hurricanes, by Kerry Emanuel, pp. 296.
714 Foreword by Kerry Emanuel. Oxford University Press, Sep 2005. ISBN-10:
715 0195149416. ISBN-13: 9780195149418,

716 Emanuel, K., C. DesAutels, C. Holloway, and R. Korty, 2004: Environmental Control
717 of Tropical Cyclone Intensity. *Journal of the Atmospheric Sciences*, 61, 843-858.

718 Fraedrich, K. and L. M. Leslie, 1989: Estimates of Cyclone Track Predictability .1.
719 Tropical Cyclones in the Australian Region. *Quarterly Journal of the Royal*
720 *Meteorological Society*, 115, 79-92.

721 Fu, B., M. S. Peng, T. Li, and D. E. Stevens, 2011: Developing versus Nondeveloping
722 Disturbances for Tropical Cyclone Formation. Part II: Western North Pacific.
723 *Monthly Weather Review*, 140, 1067-1080.

724 Fudeyasu, H., S. Iizuka, and T. Matsuura, 2006: Impact of ENSO on landfall
725 characteristics of tropical cyclones over the western North Pacific during the
726 summer monsoon season. *Geophysical research letters*, 33.

727 George, J. E., and W. M. Gray, 1977: Tropical cyclone recurvature and nonrecurvature
728 as related to surrounding wind-height fields. *J. Appl. Meteor.*, 16, 34-42.

729 Gray, W. M., 1979: Hurricanes: Their formation, structure and likely role in the
730 tropical circulation. *Meteorology over the tropical oceans*, 155-218.

731 Gray, W. M., 1998: The formation of tropical cyclones. *Meteorology and Atmospheric*
732 *Physics*, 67, 37-69.

733 Harr, P. A. and R. L. Elsberry, 1991: Tropical Cyclone Track Characteristics as a
734 Function of Large-Scale Circulation Anomalies. *Monthly Weather Review*, 119,
735 1448-1468.

736 Holland, G. J. and M. Lander, 1993: The Meandering Nature of Tropical Cyclone
737 Tracks. *Journal of the Atmospheric Sciences*, 50, 1254-1266.

738 Hong, C.-C., Y.-H. Li, T. Li, and M.-Y. Lee, 2011: Impacts of central Pacific and
739 eastern Pacific El Niños on tropical cyclone tracks over the western North Pacific.
740 *Geophys. Res. Lett.*, 38, L16712.

741 Iizuka, S. and T. Matsuura, 2008: ENSO and Western North Pacific tropical cyclone
742 activity simulated in a CGCM. *Climate Dynamics*, 30, 815-830.

743 Jia, L., X. Yang, G. A. Vecchi, R. G. Gudgel, T. L. Delworth, A. Rosati, W. F. Stern, A.
744 T. Wittenberg, L. Krishnamurthy, S. Zhang, R. Msadek, S. Kapnick, S.
745 Underwood, F. Zeng, W. G. Anderson, V. Balaji, and K. Dixon, 2015.a: Improved

746 Seasonal Prediction of Temperature and Precipitation over Land in a
747 High-Resolution GFDL Climate Model. *Journal of Climate*, 28, 2044-2062.

748 Jia, L.; G.A. Vecchi; X. Yang; R. Gudgel; T. Delworth; W. Stern; K. Paffendorf; S.
749 Underwood; F. Zeng, 2015.b: The Roles of Radiative Forcing, Sea Surface
750 Temperatures, and Atmospheric and Land Initial Conditions in U.S. Summer
751 Warming Episodes. *J. Climate* (submitted).

752 Kalnay, E., M. Kanamitsu, R. Kistler, W. Collins, D. Deaven, L. Gandin, M. Iredell, S.
753 Saha, G. White, and J. Woollen, 1996: The NCEP/NCAR 40-year reanalysis
754 project. *Bulletin of the American Meteorological Society*, 77, 437-471.

755 Kim, H.-S., G. A. Vecchi, T. R. Knutson, W. G. Anderson, T. L. Delworth, A. Rosati, F.
756 Zeng, and M. Zhao, 2014: Tropical Cyclone Simulation and Response to CO2
757 Doubling in the GFDL CM2.5 High-Resolution Coupled Climate Model. *Journal*
758 *of Climate*, 27, 8034-8054.

759 Kim, H. M., P. J. Webster, and J. A. Curry, 2009: Impact of shifting patterns of Pacific
760 Ocean warming on North Atlantic tropical cyclones. *Science*, 325, 77.

761 Kirtman, B. P. and coauthors, 2014: The North American multimodel ensemble:
762 Phase-1 Seasonal-to-interannual prediction; Phase-2 toward developing
763 intraseasonal prediction. *Bull. Amer. Meteor. Soc.*, **95**, 585–601.

764 Knapp, K. R., M. C. Kruk, D. H. Levinson, H. J. Diamond, and C. J. Neumann, 2010:
765 The International Best Track Archive for Climate Stewardship (IBTrACS).
766 *Bulletin of the American Meteorological Society*, 91, 363-376.

767 Kobayashi, S., Y. Ota, Y. Harada, A. Ebita, M. Moriya, H. Onoda, K. Onogi, H.
768 Kamahori, C. Kobayashi, H. Endo, K. Miyaoka, and K. Takahashi, 2015: The
769 JRA-55 Reanalysis: General Specifications and Basic Characteristics. *Journal of*
770 *the Meteorological Society of Japan. Ser. II*, 93, 5-48.

771 Krishnamurthy, L., G. Vecchi; R. Msadek; A. Wittenberg; T. Delworth; F. Zeng,
772 2015.a: The Seasonality of the Great Plains Low-Level Jet and ENSO
773 Relationship. *J. Climate*. doi:10.1175/JCLI-D-14-00590.1

774 Krishnamurthy, L and coauthors, 2015.b: Effect of extreme ENSO events on regional
775 tropical cyclone activity in high-resolution model. *J. Climate*, submitted.

776 Lau, K. M. and S. Yang, 1996: Seasonal variation, abrupt transition, and intraseasonal
777 variability associated with the Asian summer monsoon in the GLA GCM. *Journal*
778 *of Climate*, 9, 965-985.

779 Lau, N.-C. and M. J. Nath, 1996: The Role of the atmospheric Bridge in Linking
780 Tropical Pacific ENSO Events to Extratropical SST Anomalies. *Journal of*
781 *Climate*, 9, 2036-2057.

782 —, 1996: The Role of the "atmospheric Bridge" in Linking Tropical Pacific ENSO
783 Events to Extratropical SST Anomalies. *Journal of Climate*, 9, 2036-2057.

784 Li, C. and C. Wang, 2014: Simulated impacts of two types of ENSO events on
785 tropical cyclone activity in the western North Pacific: large-scale atmospheric
786 response. *Climate Dynamics*, 42, 2727-2743.

787 Li, R. C. and W. Zhou, 2012: Changes in western Pacific tropical cyclones associated
788 with the El Niño-southern oscillation cycle. *Journal of Climate*, 25, 5864-5878.

789 Lyons, S. W., 2004: US tropical cyclone landfall variability: 1950-2002. *Weather and*
790 *Forecasting*, 19, 473-480.

791 Msadek, R., G.A. Vecchi, M. Winton, R.G. Gudgel (2014): Importance of initial
792 conditions in seasonal predictions of Arctic sea ice extent. *Geophys. Res. Lett.*
793 DOI: 10.1002/2014GL060799

794 Murakami, H. and B. Wang, 2010: Future Change of North Atlantic Tropical Cyclone
795 Tracks: Projection by a 20-km-Mesh Global Atmospheric Model. *Journal of*
796 *Climate*, 23, 2699-2721.

797 Murakami, H. and M. Sugi, 2010: Effect of Model Resolution on Tropical Cyclone
798 Climate Projections. *SOLA*, 6, 73-76.

799 Murakami, H., B. Wang, and A. Kitoh, 2011: Future Change of Western North Pacific
800 Typhoons: Projections by a 20-km-Mesh Global Atmospheric Model. *Journal of*
801 *Climate*, 24, 1154-1169.

802 Murakami, H., G. A. Vecchi, S. Underwood, T. Delworth, A. T. Wittenberg,
803 W. Anderson, J. -H. Chen, R. Gudgel, L. Harris, S. -J. Lin, and F. Zeng,
804 2015: Simulation and prediction of Category 4 and 5 hurricanes in the
805 high-resolution GFDL HiFLOR coupled climate model. *J. Climate*, in press

806 Philander, S. G. H., 1983: El-Niño Southern Oscillation Phenomena. *Nature*, 302,
807 295-301.

808 Pielke Jr, R., J. Gratz, C. Landsea, D. Collins, M. Saunders, and R. Musulin, 2008:
809 Normalized hurricane damage in the United States: 1900–2005. *Natural Hazards*
810 *Review*, 9, 29.

811 Peduzzi, P., B. Chatenoux, H. Dao, A. De Bono, C. Herold, J. Kossin, F. Mouton, and
812 O. Nordbeck, 2012: Global trends in tropical cyclone risk. *Nature Climate Change*,
813 2, 289-294.

814 Rasmusson, E. M. and T. H. Carpenter, 1982: Variations in tropical sea surface
815 temperature and surface wind fields associated with the Southern Oscillation/El
816 Niño. *Monthly Weather Review*, 110, 354-384.

817 Rayner, N., D. E. Parker, E. Horton, C. Folland, L. Alexander, D. Rowell, E. Kent,
818 and A. Kaplan, 2003: Global analyses of sea surface temperature, sea ice, and
819 night marine air temperature since the late nineteenth century. *Journal of*
820 *Geophysical Research: Atmospheres* (1984–2012), 108.

821 Riehl, H., and R. J. Shafer, 1944: The recurvature of tropical storms. *J. Atmos. Sci.*, 1,
822 42–54.

823 Shaevitz, D. A., S. J. Camargo, A. H. Sobel, J. A. Jonas, D. Kim, A. Kumar, T. E.
824 LaRow, Y.-K. Lim, H. Murakami, K. A. Reed, M. J. Roberts, E. Scoccimarro, P. L.
825 Vidale, H. Wang, M. F. Wehner, M. Zhao, and N. Henderson, 2014:
826 Characteristics of tropical cyclones in high-resolution models in the present
827 climate. *Journal of Advances in Modeling Earth Systems*, 6, 1154-1172.

828 Shaffrey, L. C., I. Stevens, W. Norton, M. Roberts, P. L. Vidale, J. Harle, A. Jrrar, D.
829 Stevens, M. J. Woodage, and M.-E. Demory, 2009: UK HiGEM: The new UK
830 high-resolution global environment model-model description and basic evaluation.
831 *Journal of Climate*, 22, 1861-1896.

832 Trenberth, K. E., J. M. Caron, D. P. Stepaniak, and S. Worley, 2002: Evolution of El
833 Niño–Southern Oscillation and global atmospheric surface temperatures. *Journal*
834 *of Geophysical Research: Atmospheres*, 107, AAC 5-1-AAC 5-17.

835 Tuleya, R., M. Bender, and Y. Kurihara, 1984: A simulation study of the landfall of
836 tropical cyclones using a movable nested-mesh model. *Mon. Wea. Rev.*, 112,
837 124–136.

838 Vecchi, G. A., T. Delworth, R. Gudgel, S. Kapnick, A. Rosati, A. T. Wittenberg, F.
839 Zeng, W. Anderson, V. Balaji, K. Dixon, L. Jia, H. S. Kim, L. Krishnamurthy, R.
840 Msadek, W. F. Stern, S. D. Underwood, G. Villarini, X. Yang, and S. Zhang, 2014:
841 On the Seasonal Forecasting of Regional Tropical Cyclone Activity. *Journal of*
842 *Climate*, 27, 7994-8016.

843 Vitart, F. and J. Anderson, 2001: Sensitivity of Atlantic tropical storm frequency to
844 ENSO and interdecadal variability of SSTs in an ensemble of AGCM integrations.
845 *Journal of climate*, 14, 533-545.

846 Wang, B. and J. C. L. Chan, 2002: How strong ENSO events affect tropical storm
847 activity over the Western North Pacific. *Journal of Climate*, 15, 1643-1658.

848 Wang, H., J. Sun, and K. Fan, 2007: Relationships between the North Pacific
849 Oscillation and the typhoon/hurricane frequencies. *Science in China Series D:*
850 *Earth Sciences*, 50, 1409-1416.

851 Wang, H., L. Long, A. Kumar, W. Wang, J.-K. E. Schemm, M. Zhao, G. A. Vecchi, T.
852 E. Larow, Y.-K. Lim, S. D. Schubert, D. A. Shaevitz, S. J. Camargo, N. Henderson,
853 D. Kim, J. A. Jonas, and K. J. E. Walsh, 2014: How Well Do Global Climate
854 Models Simulate the Variability of Atlantic Tropical Cyclones Associated with
855 ENSO? *Journal of Climate*, 27, 5673-5692.

856 Wong, M. L. M. and J. C. L. Chan, 2004: Tropical cyclone intensity in vertical wind
857 shear. *Journal of the Atmospheric Sciences*, 61, 1859-1876.

858 Wu, G. X. and N. C. Lau, 1992: A Gcm Simulation of the Relationship between
859 Tropical-Storm Formation and Enso. *Monthly Weather Review*, 120, 958-977.

860 Wu, L. and B., Wang, 2000: A Potential Vorticity Tendency Diagnostic Approach for
861 Tropical Cyclone Motion. *Mon. Wea. Rev.*, 128, 1899–1911.

862 Wu, L. and B. Wang, 2001: Movement and Vertical Coupling of Adiabatic Baroclinic
863 Tropical Cyclones. *Journal of the Atmospheric Sciences*, 58, 1801-1814.

864 Wu, M., W. Chang, and W. Leung, 2004: Impacts of El Niño-Southern Oscillation
865 events on tropical cyclone landfalling activity in the western North Pacific.
866 *Journal of Climate*, 17, 1419-1428.

867 Wunsch, C., 1991: Large-Scale Response of the Ocean to Atmospheric Forcing at
868 Low-Frequencies. *Journal of Geophysical Research-Oceans*, 96, 15083-15092.

869 Yang, X., G. A. Vecchi, R. G. Gudgel, T. L. Delworth, S. Zhang, A. Rosati, L. Jia, W.
870 F. Stern, A. T. Wittenberg, S. Kapnick, R. Msadek, S. D. Underwood, F. Zeng, W.
871 Anderson, and V. Balaji, 2015.a: Seasonal predictability of extratropical storm
872 tracks in GFDL's high-resolution climate prediction model. *Journal of Climate*.
873 Yang, X., G. A. Vecchi, T. L. Delworth, K. Paffendorf, R. Gudgel, L. Jia, Seth
874 D. Underwood, and F. Zeng, 2015.b: Extreme North America winter storm season
875 of 2013-14: Roles of Radiative Forcing, the Global Warming Hiatus and Internal
876 Variability. *Bull. Amer. Meteorol. Soc.* (in press).
877 Zehr, R. M., 1992: Tropical cyclogenesis in the western North Pacific. PhD thesis,
878 Colorado State University.
879 Zhang, Q., Q. Liu, and L. Wu, 2009: Tropical Cyclone Damages in China 1983–2006.
880 *Bulletin of the American Meteorological Society*, **90**, 489-495.
881 Zhang, W., H. F. Graf, Y. Leung, and M. Herzog, 2012: Different El Niño Types and
882 Tropical Cyclone Landfall in East Asia. *Journal of Climate*, 25, 6510-6523.
883 Zhang, W., Y. Leung, and K. Fraedrich, 2015a: Different El Niño types and intense
884 typhoons in the Western North Pacific. *Climate Dynamics*, 11-12, 2965-2977 .
885 Zhang, W., G., Vecchi, G., Villarini, Murakami, H., and L. Jia, 2015b: The Pacific
886 Meridional Mode and the Occurrence of Tropical Cyclones in the Western North
887 Pacific, *Journal of Climate*, (accepted).
888 Zhao, M., I. M. Held, and G. A. Vecchi, 2010: Retrospective Forecasts of the
889 Hurricane Season Using a Global Atmospheric Model Assuming Persistence of
890 SST Anomalies. *Monthly Weather Review*, 138, 3858-3868.
891
892
893

894 Table 1. Classification of El Niño and La Niña years for the period of 1961-2013
 895 based on the Niño3.4 index.

El Niño	La Niña
1963, 1965, 1969, 1972, 1976, 1982, 1987, and 1997	1964, 1970, 1973, 1975, 1988, 1999, 2007 and 2010

896

897

898

899

900 Table 2. The standard deviation of Niño3.4 index in the first 300 years of the control

901 experiments with HiFLOR, FLOR and observations (53 years).

Magnitude	HiFLOR	FLOR	Observations
Niño3.4	0.78	1.31	0.79

902

903

904 Table 3. Correlation coefficients between TC landfall over Japan&Korea, the
 905 Philippines, ICMP, China and East Asia and the Niño3.4 index based on observations,
 906 and the SST-restoring experiments with HiFLOR and FLOR for the period of
 907 1971-2012. The symbols ***, ** and * indicate results that are significant at the
 908 levels of 0.01, 0.05 and 0.1, respectively.

909

TC-landfall Correlation	IBTrACS	FLOR (SST Restoring)	HiFLOR (SST Restoring)
Japan & Korea	-0.02	-0.07	-0.16
Philippines	-0.24*	-0.28**	-0.41***
ICMP	-0.30**	-0.12	-0.51***
China	-0.49***	0.32**	-0.38***
East Asia	-0.27**	0.03	-0.61***

910

911

912 **Figure captions**

913 Figure 1. TC density climatology in the control experiments (300 years) of HiFLOR,
914 FLOR and observations (1961-2013).

915 Figure 2. TC genesis climatology in the control experiments (300 years) of HiFLOR,
916 FLOR and observations (1961-2013). The red plus sign represents the mean TC
917 genesis location.

918 Figure 3. TC track density anomalies (units: times/year; binned into $5^\circ \times 5^\circ$ grid box)
919 in the WNP during El Niño and La Niña phases based on HiFLOR (a,b), FLOR (c,d)
920 and observations (e,f).

921 Figure 4. Regressions of TC track density (units: times/year; binned into $5^\circ \times 5^\circ$ grid
922 box) onto Niño3.4 based on the control experiments with HiFLOR (a) and FLOR (b)
923 and observations (c).

924 Figure 5. TC genesis anomalies (units: times/year; binned into $5^\circ \times 5^\circ$ grid box) in the
925 WNP during El Niño and La Niña phases based on the control experiments with
926 HiFLOR (a,b), FLOR (c,d) and observations (e,f).

927 Figure 6. Correlation between Niño3.4 and TC landfall frequency over Japan and
928 Korea, the Philippines, the Indochina and Malay Peninsula (ICMP), China, and East
929 Asia in the 300-yr control experiments of FLOR and HiFLOR and in the observations.
930 The correlation for HiFLOR and FLOR are calculated by averaging the correlation
931 coefficients for every 53-year moving periods and the error bars represent the
932 confidence interval of the average correlation coefficients for each 53-year periods at
933 0.05 level of significance.

934 Figure 7. SST (unit: $^\circ\text{C}$) anomalies during El Niño and La Niña phases based on
935 control experiments with observations (a,b), HiFLOR - observations (c,d) and FLOR -
936 observations (e,f).

937 Figure 8. Precipitation anomalies (unit: mm/day, PreAno) during El Niño and La Niña
938 phases based on observations (a,b), HiFLOR - observations (c,d) and FLOR -
939 observations (e,f).

940 Figure 9. Vertical profile of wind vector (zonal wind (averaged over 5°N to 20°N)
941 and $-50 \cdot \omega$ (unit: pa/s)) during El Niño and La Niña phases based on observations
942 (a,b), HiFLOR - observations (c,d) and FLOR - observations (e,f). The shading in this
943 figure represents ω (omega).

944 Figure 10. Differences in steering flow (unit: ms^{-1}) (HiFLOR minus FLOR) in the
945 control experiments during El Niño (a) and La Niña (b) years. Contours represent the
946 annual average TC genesis density in the control experiment of HiFLOR.

947 Figure 11. The simulated TC density climatology in the SSS- and SST-nudging
948 experiments of HiFLOR, FLOR and observations (1971-2012).

949 Figure 12. The simulated TC genesis climatology in the SSS- and SST-nudging
950 experiments of HiFLOR, FLOR and observations (1971-2012). The red plus sign
951 represents the mean TC genesis location.

952 Figure 13. TC track density anomalies (units: times/year; binned into $5^\circ \times 5^\circ$ grid box)
953 in El Niño and La Niña events in the SST-restoring experiments of HiFLOR and
954 FLOR and the observations.

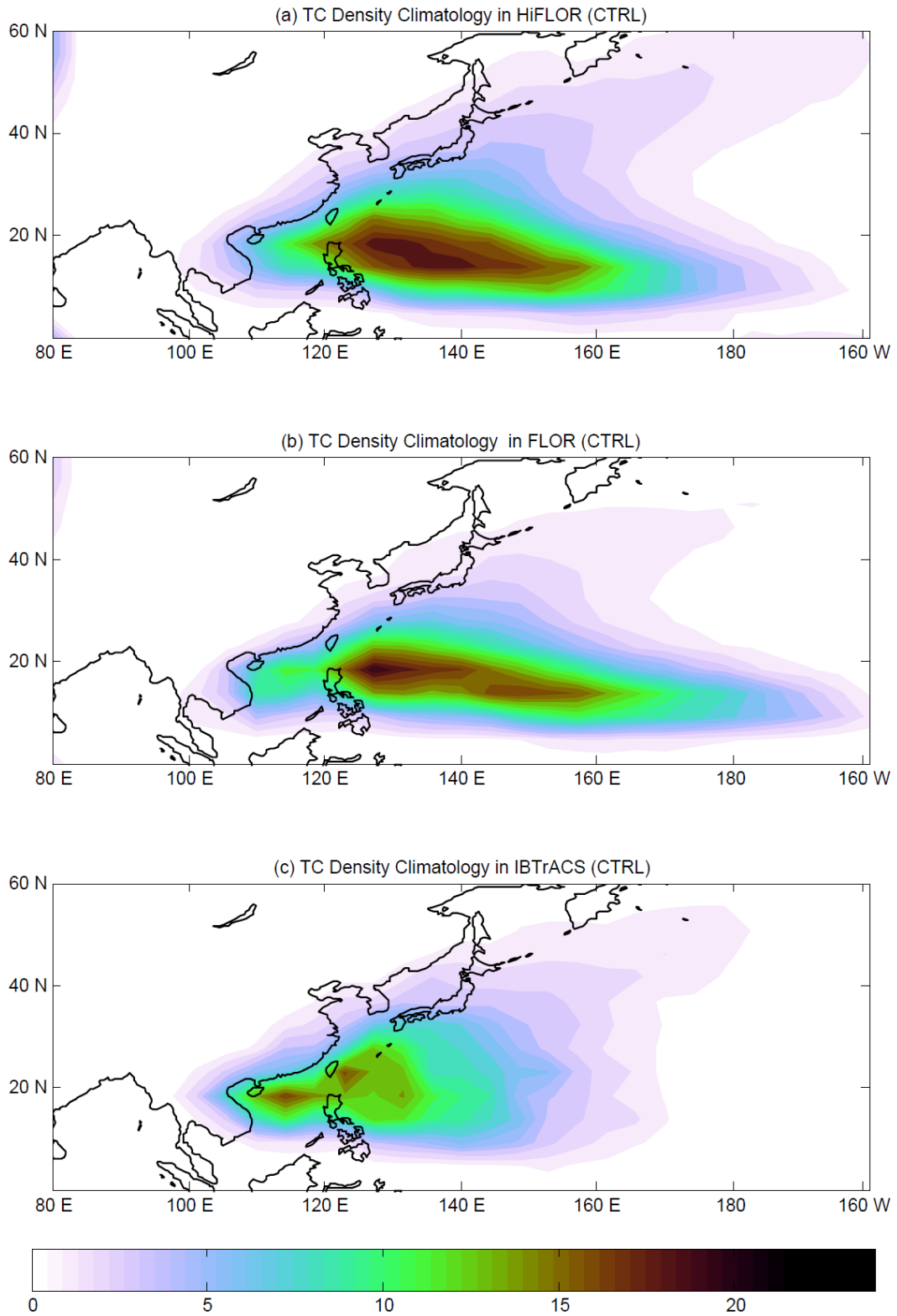
955 Figure 14. Annual average TC genesis anomalies (units: times/year; binned into $5^\circ \times 5^\circ$
956 grid box) during El Niño and La Niña events in SST-restoring experiments with
957 HiFLOR, FLOR and observations.

958 Figure 15. Precipitation anomalies (unit: mm/day) during El Niño and La Niña phases
959 based on observations (a,b), SST-restoring HiFLOR-observations (c,d) and
960 SST-restoring FLOR-observations (e, f).

961 Figure 16. Vertical profile of wind vector (zonal wind (averaged over 5°N to 20°N)
962 and $-50 \cdot \omega$ (unit: pa/s)) during El Niño and La Niña phases based on observations
963 (a,b), SST-restoring HiFLOR-observations (c,d) and SST-restoring
964 FLOR-observations (e, f) to depict the Walker circulation. "OBS" represents
965 observations. The shading in this figure represents ω (omega).

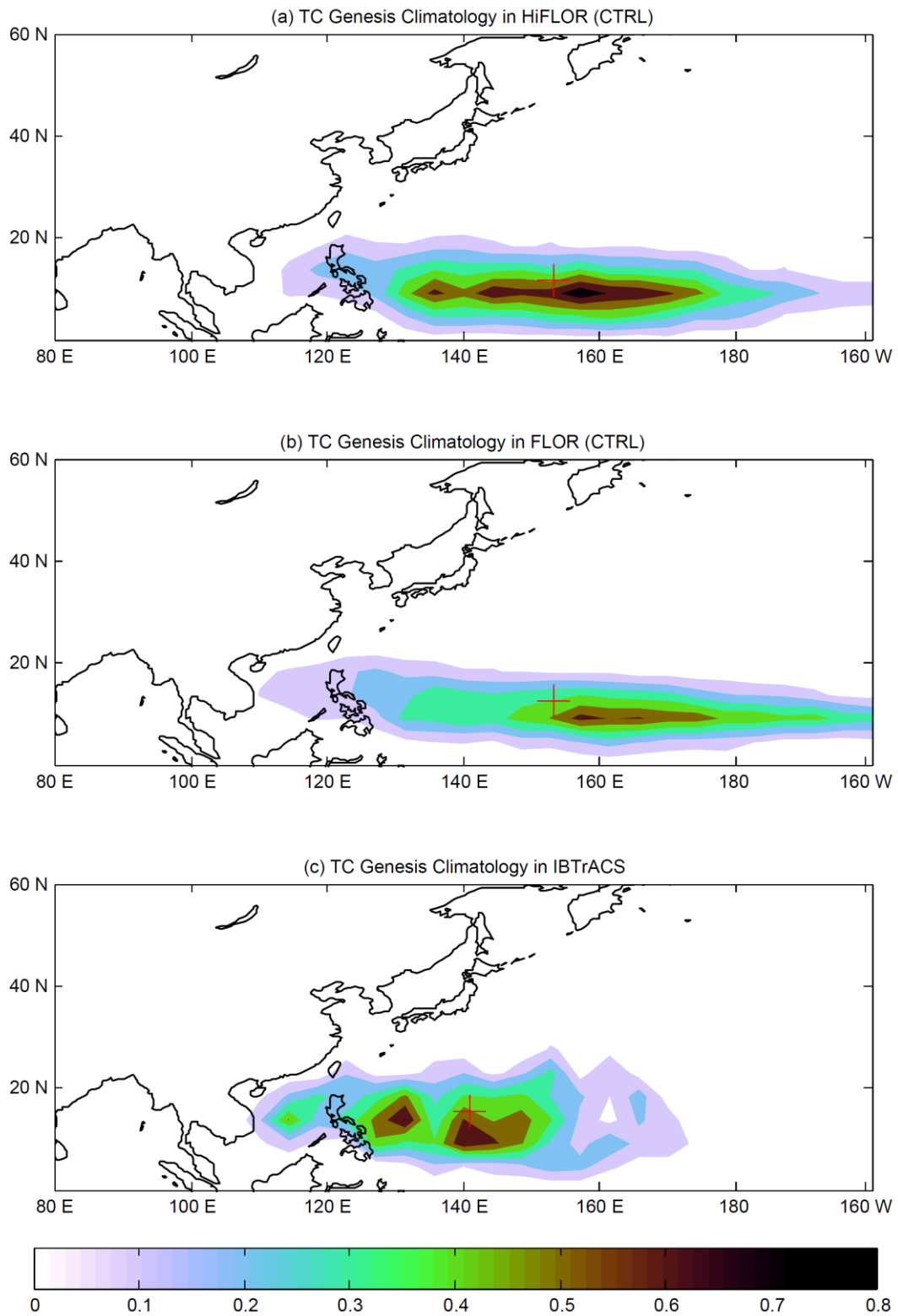
966 Figure 17. Steering flow (unit: ms^{-1}) (HiFLOR minus FLOR) in the SST-restoring
967 experiments during the El Niño (a) and La Niña (b) phase. Contours represent the
968 annual average TC genesis density in HiFLOR.

969
970
971

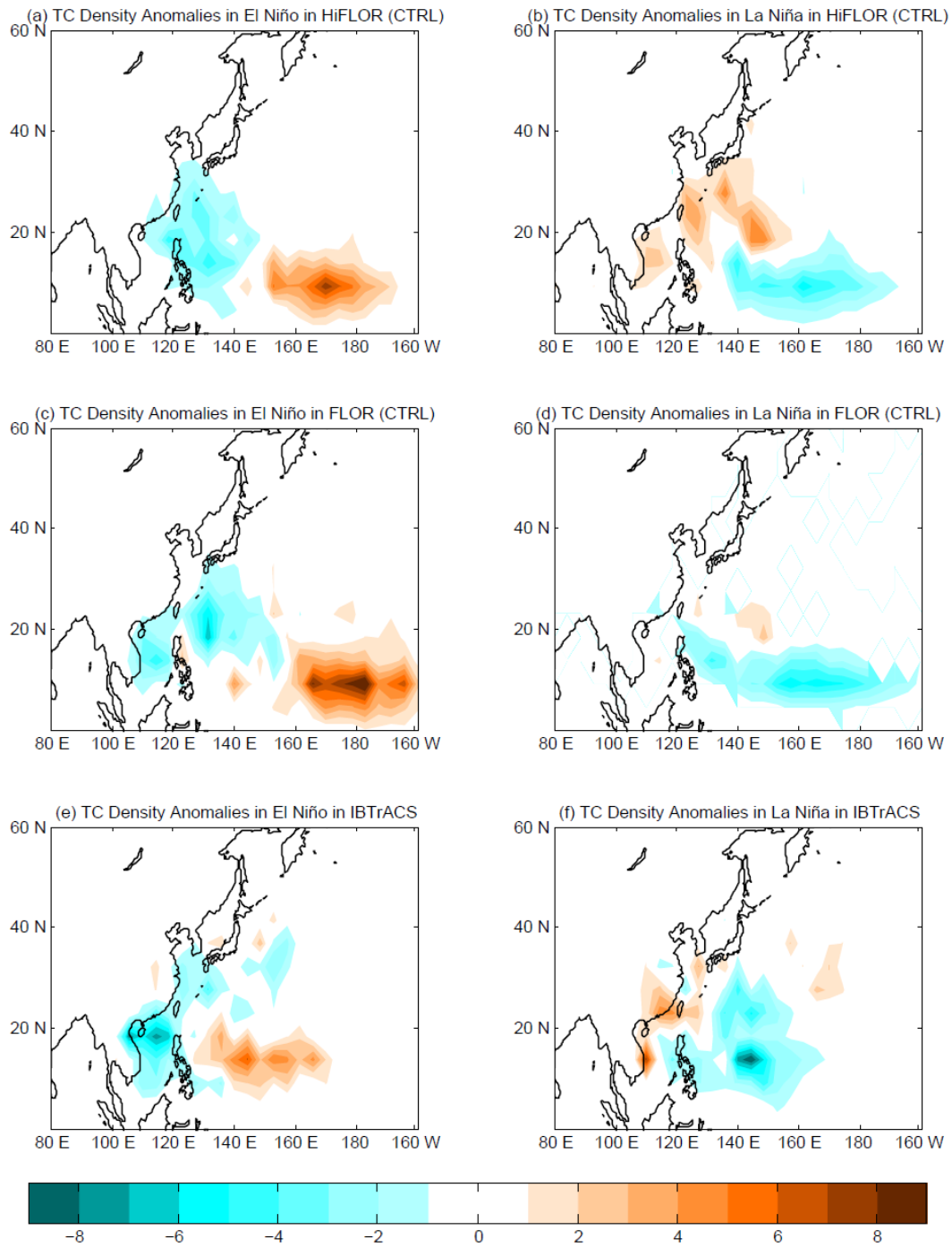


972
973
974
975

Figure 1. TC density (unit: times/year) climatology in the control experiments (300 years) of HiFLOr, FLOR and observations (1961-2013).

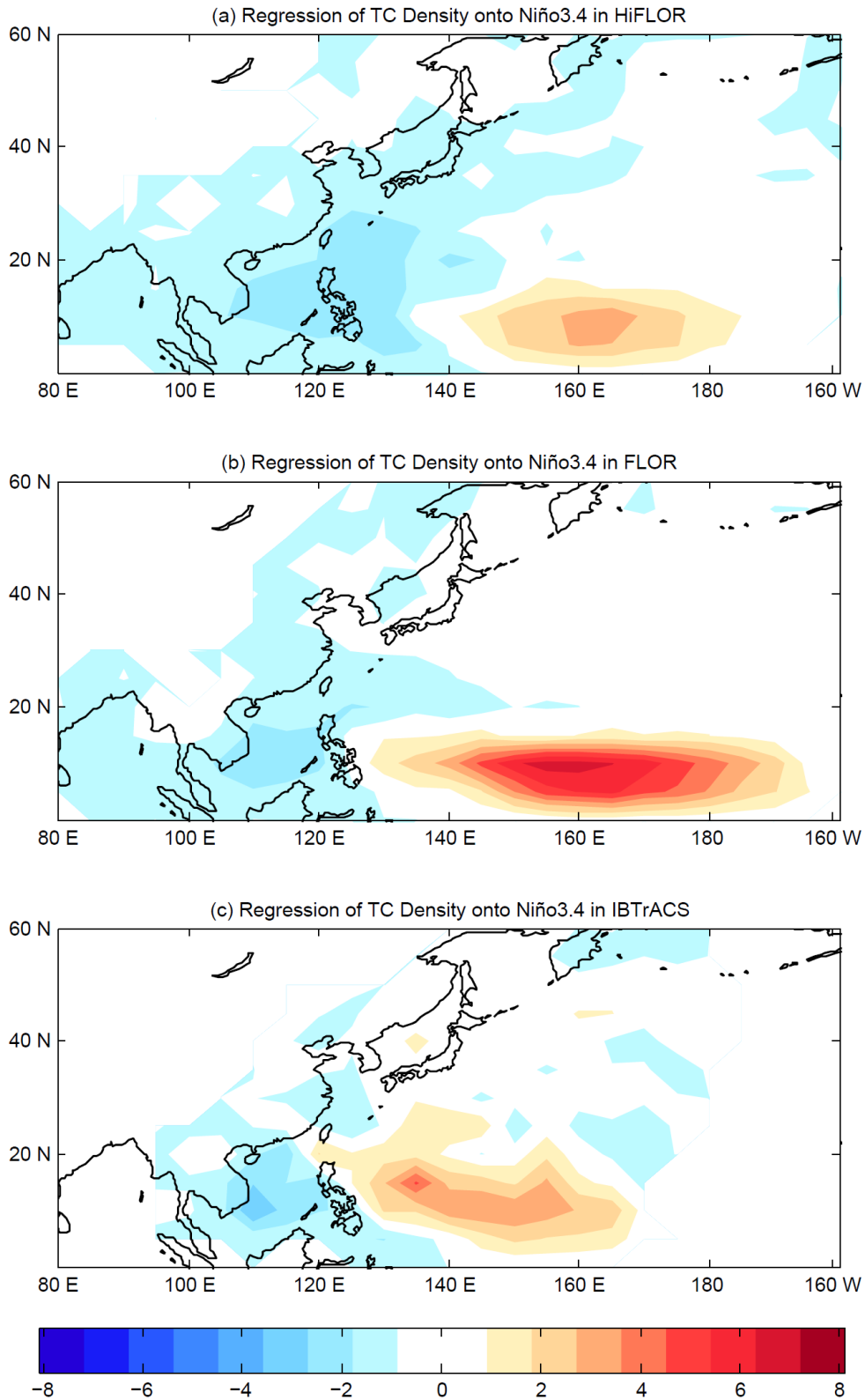


976
 977 Figure 2. TC genesis (unit: times/year) climatology in the control experiments (300
 978 years) of HiFLOR, FLOR and observations (1961-2013). The red plus sign represents
 979 the mean TC genesis location.
 980



981

982 Figure 3. TC track density anomalies (units: times/year; binned into $5^\circ \times 5^\circ$ grid box)
 983 in the WNP during El Niño and La Niña phases based on HiFLOOR (a,b), FLOR (c,d)
 984 and observations (e,f).
 985



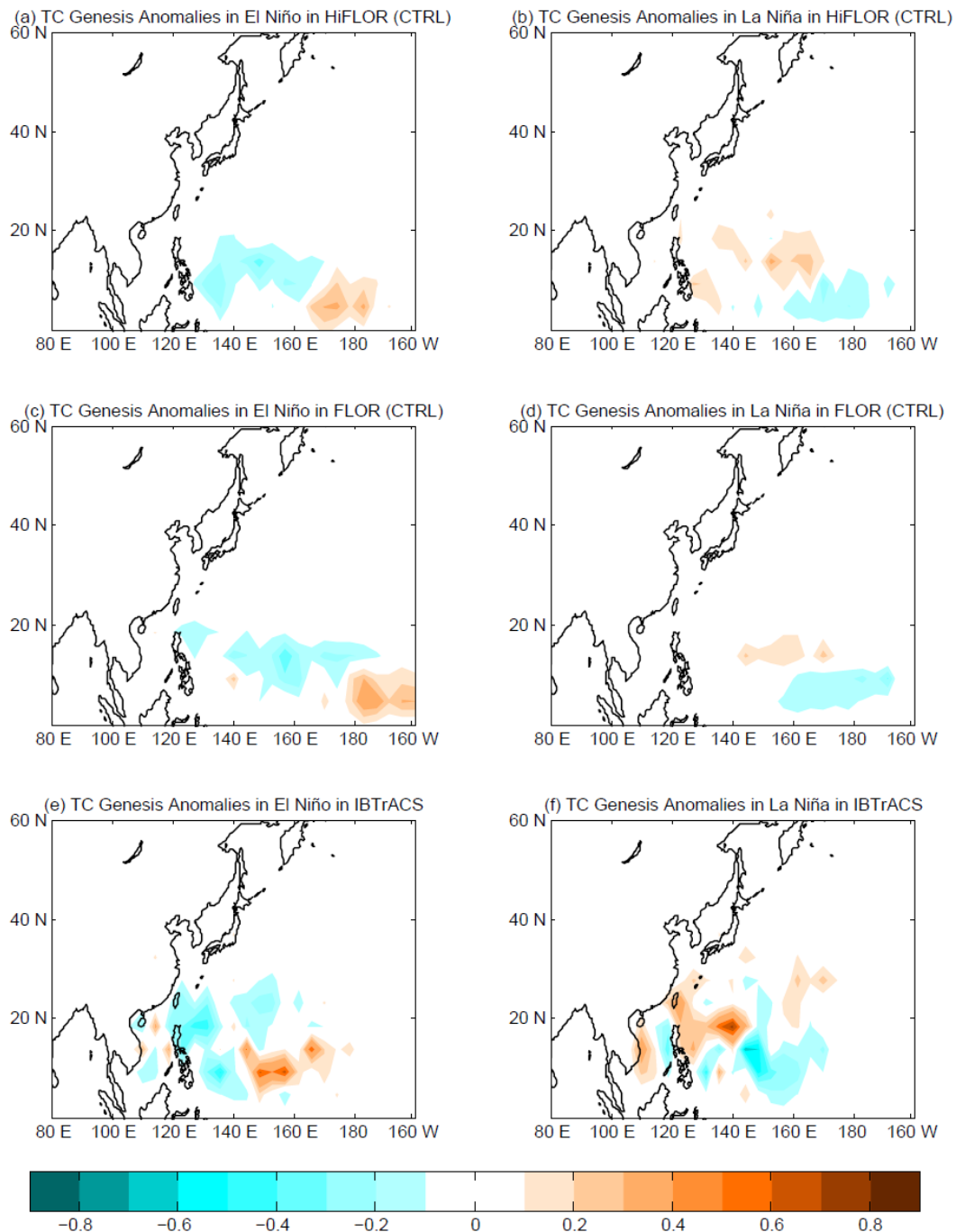
986

987 Figure 4. Regressions of TC track density (units: times/year; binned into $5^{\circ} \times 5^{\circ}$ grid

988 box) onto Niño3.4 based on the control experiments with HiFLOOR (a) and FLOR (b)

989 and observations (c).

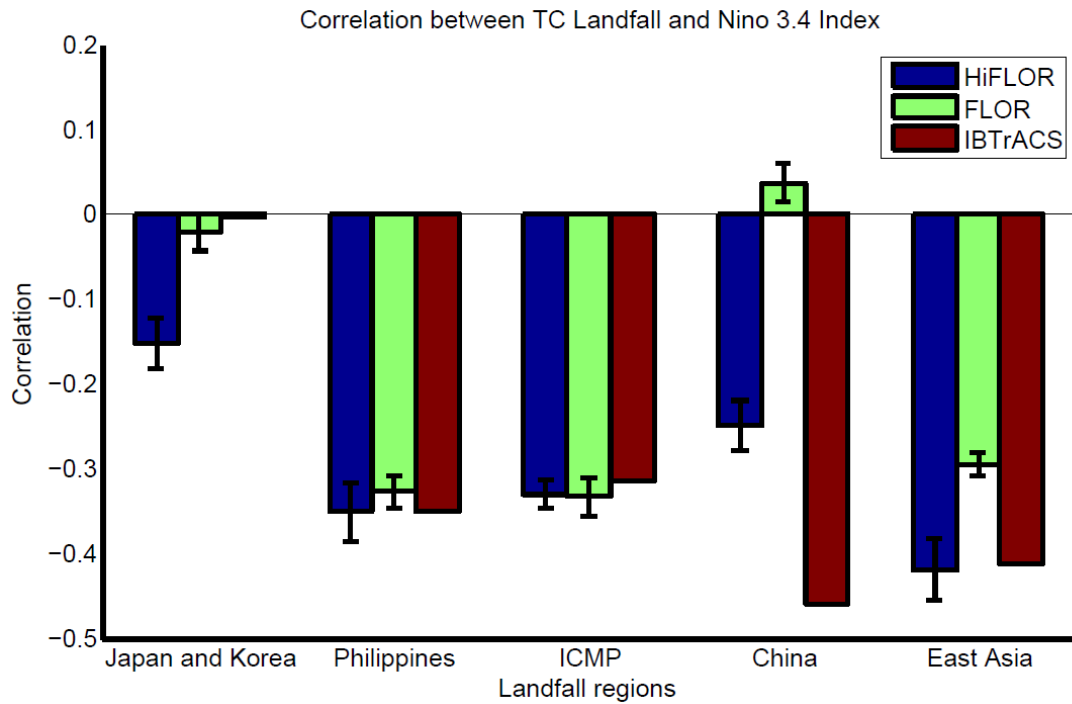
990



991

992 Figure 5. TC genesis anomalies (units: times/year; binned into $5^\circ \times 5^\circ$ grid box) in the
 993 WNP during El Niño and La Niña phases based on the control experiments with
 994 HiFLOR (a,b), FLOR (c,d) and observations (e,f).

995

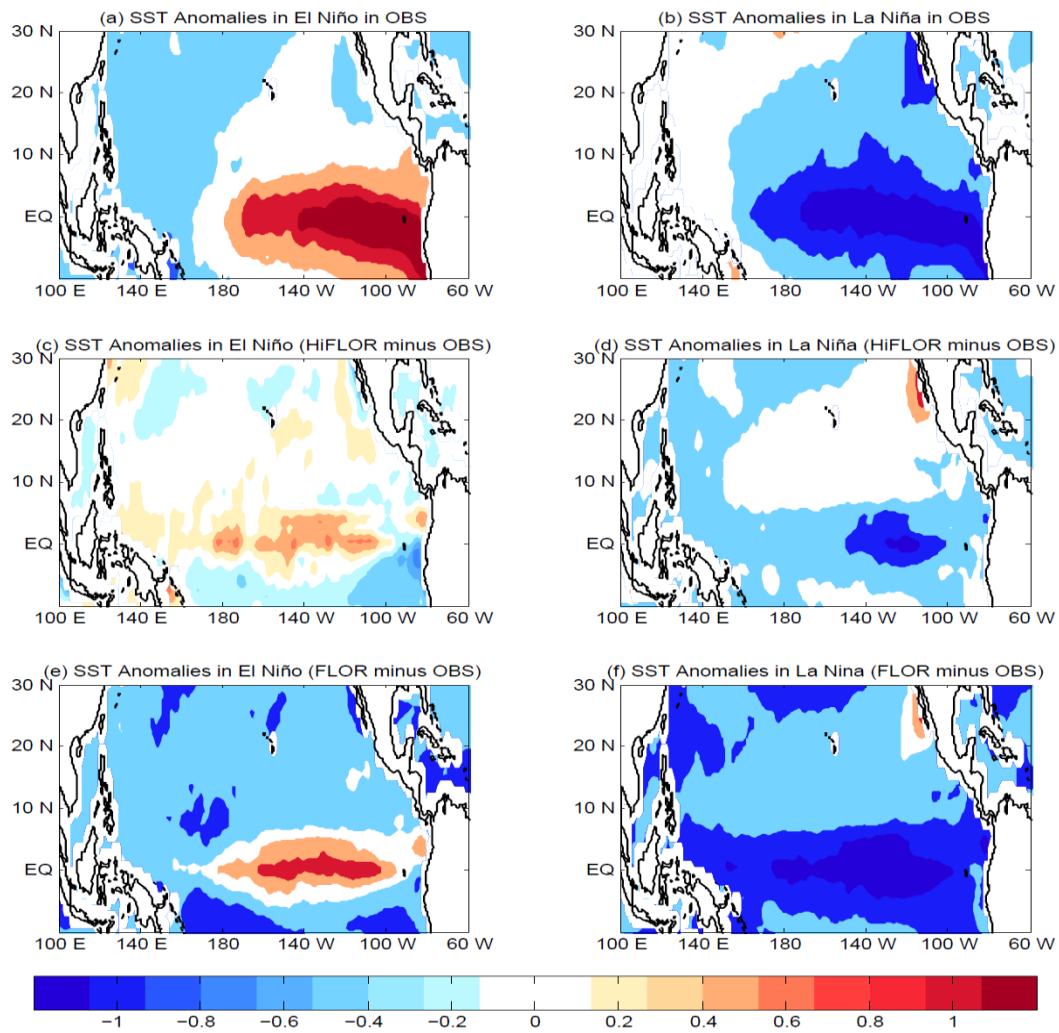


996

997 Figure 6. Correlation between Niño3.4 and TC landfall frequency over Japan and
 998 Korea, the Philippines, the Indochina and Malay Peninsula (ICMP), China, and East
 999 Asia in the 300-yr control experiments of FLOR and HiFLOR and in the observations.

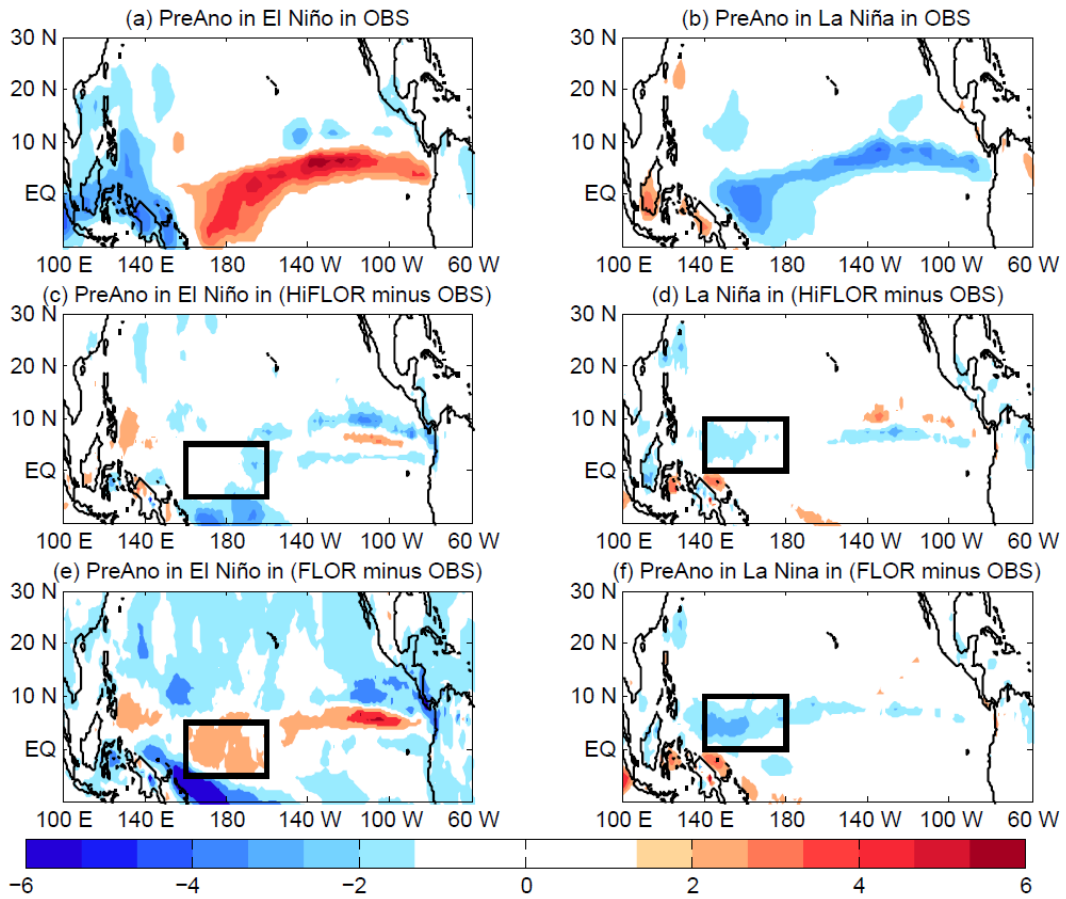
1000 The correlation for HiFLOR and FLOR are calculated by averaging the correlation
 1001 coefficients for every 53-year moving periods and the error bars represent the
 1002 confidence interval of the average correlation coefficients for each 53-year periods at
 1003 0.05 level of significance. The observations cover the period 1961-2013.

1004



1005
 1006
 1007
 1008
 1009

Figure 7. SST (unit: °C) anomalies during El Niño and La Niña phases based on control experiments with observations (a,b), HiFLOr - observations (c,d) and FLOR - observations (e,f).



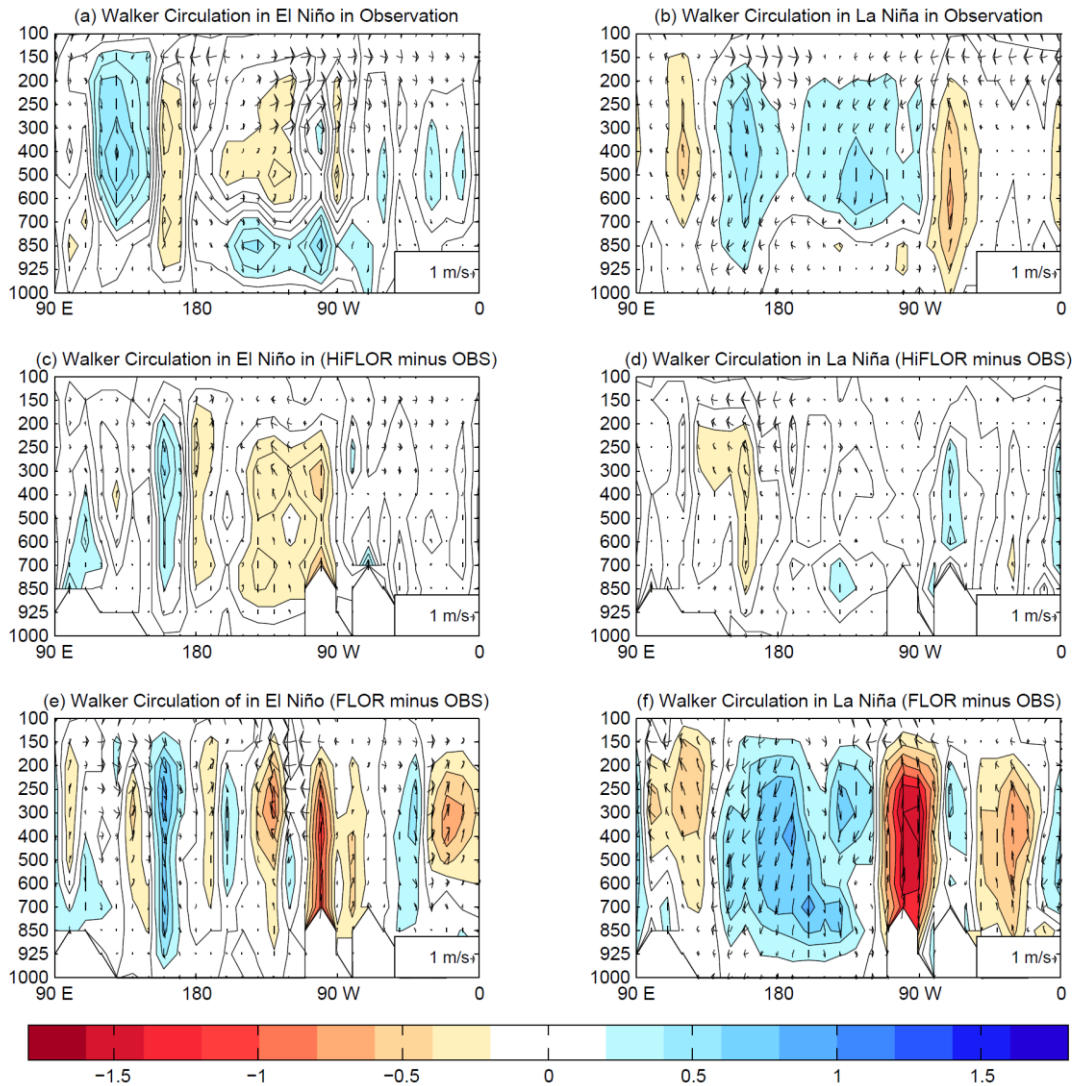
1010

1011

1012

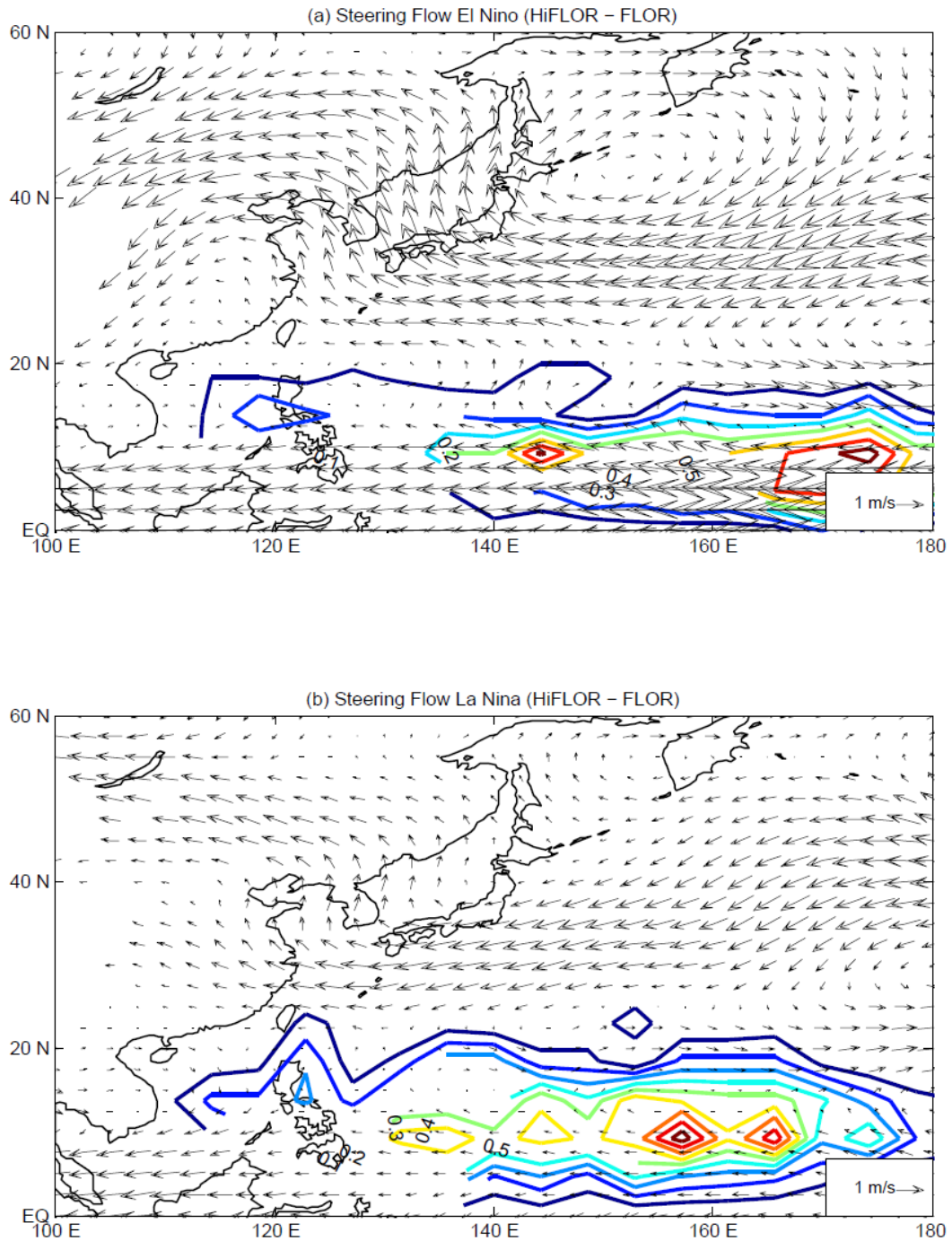
1013

Figure 8. Precipitation anomalies (unit: mm/day, PreAno) during El Niño and La Niña phases based on observations (a,b), HiFLOr - observations (c,d) and FLOR - observations (e,f).

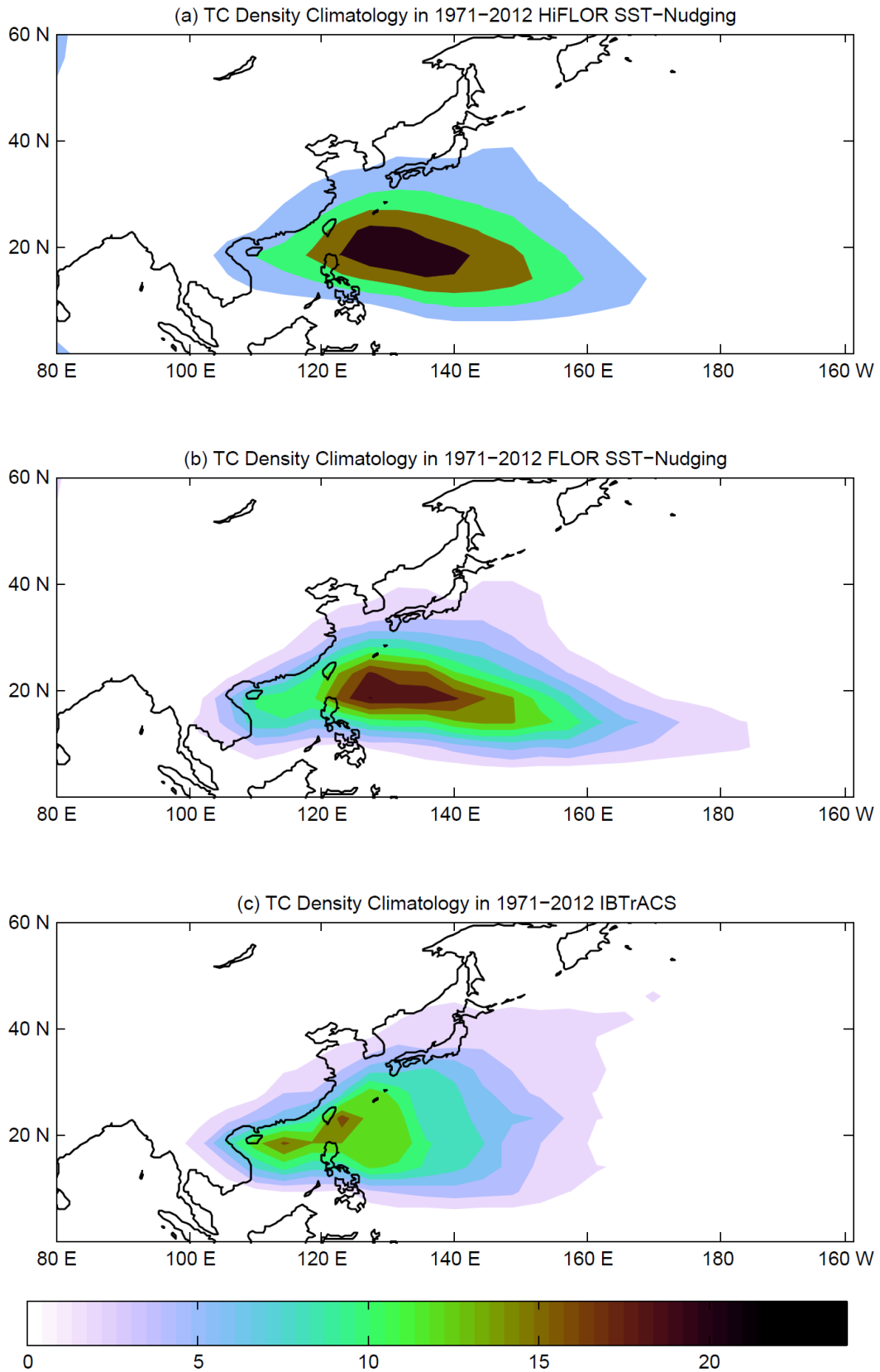


1014

1015 Figure 9. Vertical profile of wind vector [zonal wind (averaged over 5°N to 20°N) and
 1016 $-50 \cdot \omega$ (unit: pa/s)] during El Niño and La Niña phases based on observations (a,b),
 1017 HiFLOR - observations (c,d) and FLOR - observations (e,f).The shading in this figure
 1018 represents ω (omega).
 1019

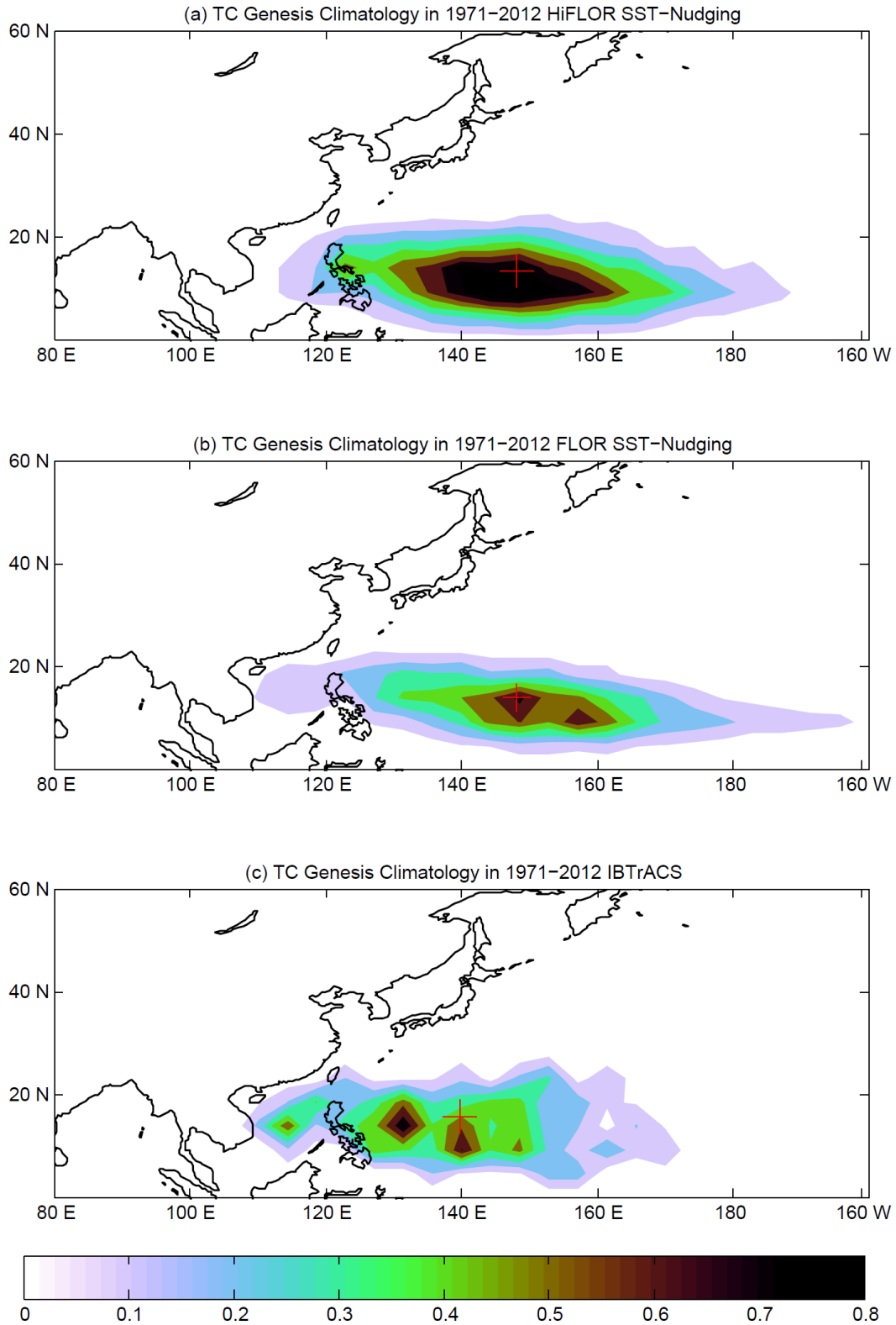


1020
 1021 Figure 10. Differences in steering flow (unit: ms^{-1}) (HiFLOOR minus FLOR) in the
 1022 control experiments during El Niño (a) and La Niña (b) years. Contours represent the
 1023 annual average TC genesis density in the control experiment of HiFLOOR.
 1024



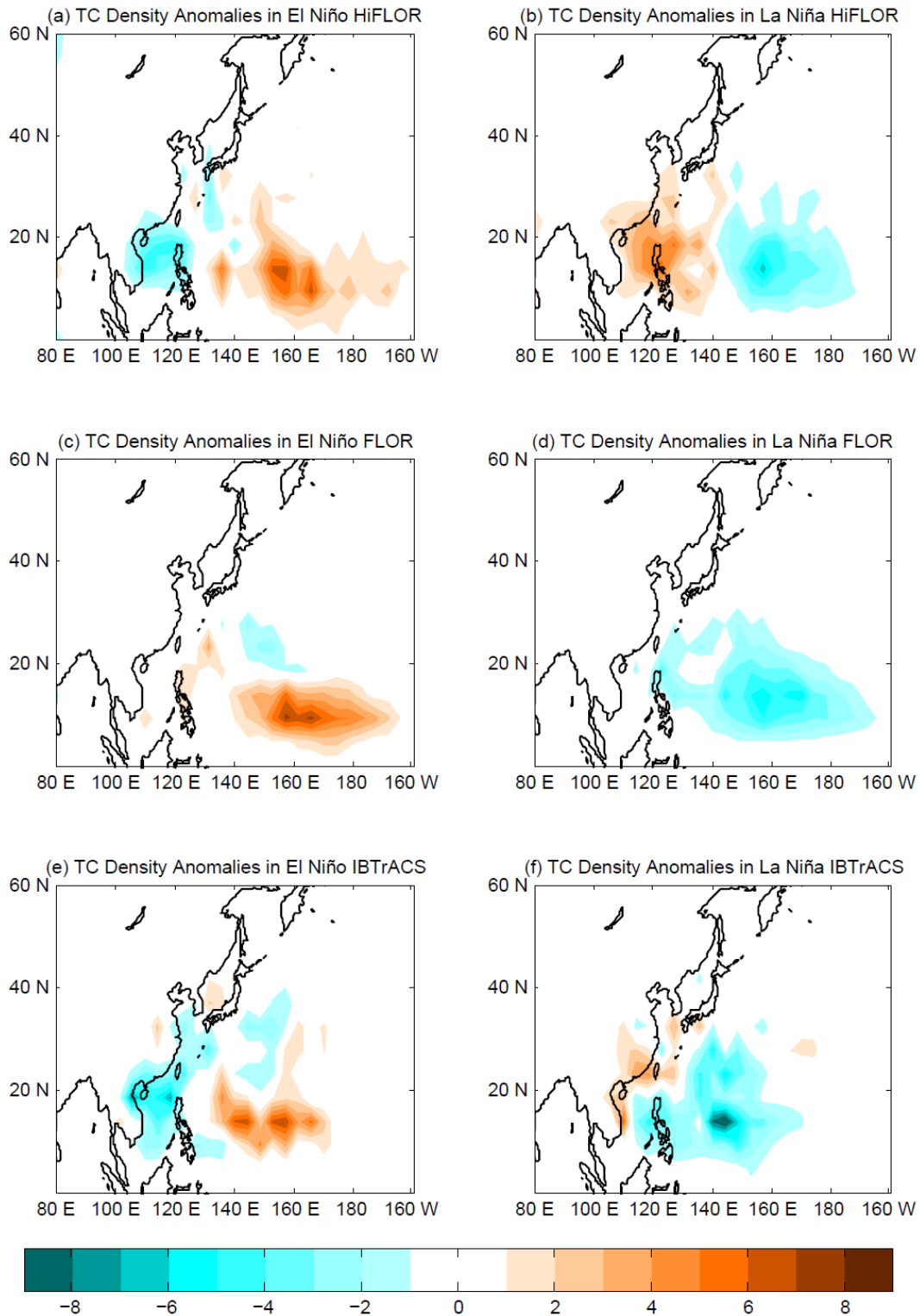
1025
 1026
 1027
 1028

Figure 11. The simulated TC density (unit: times/year) climatology in the SSS- and SST-nudging experiments of HiFLOr, FLOR and observations (1971-2012).



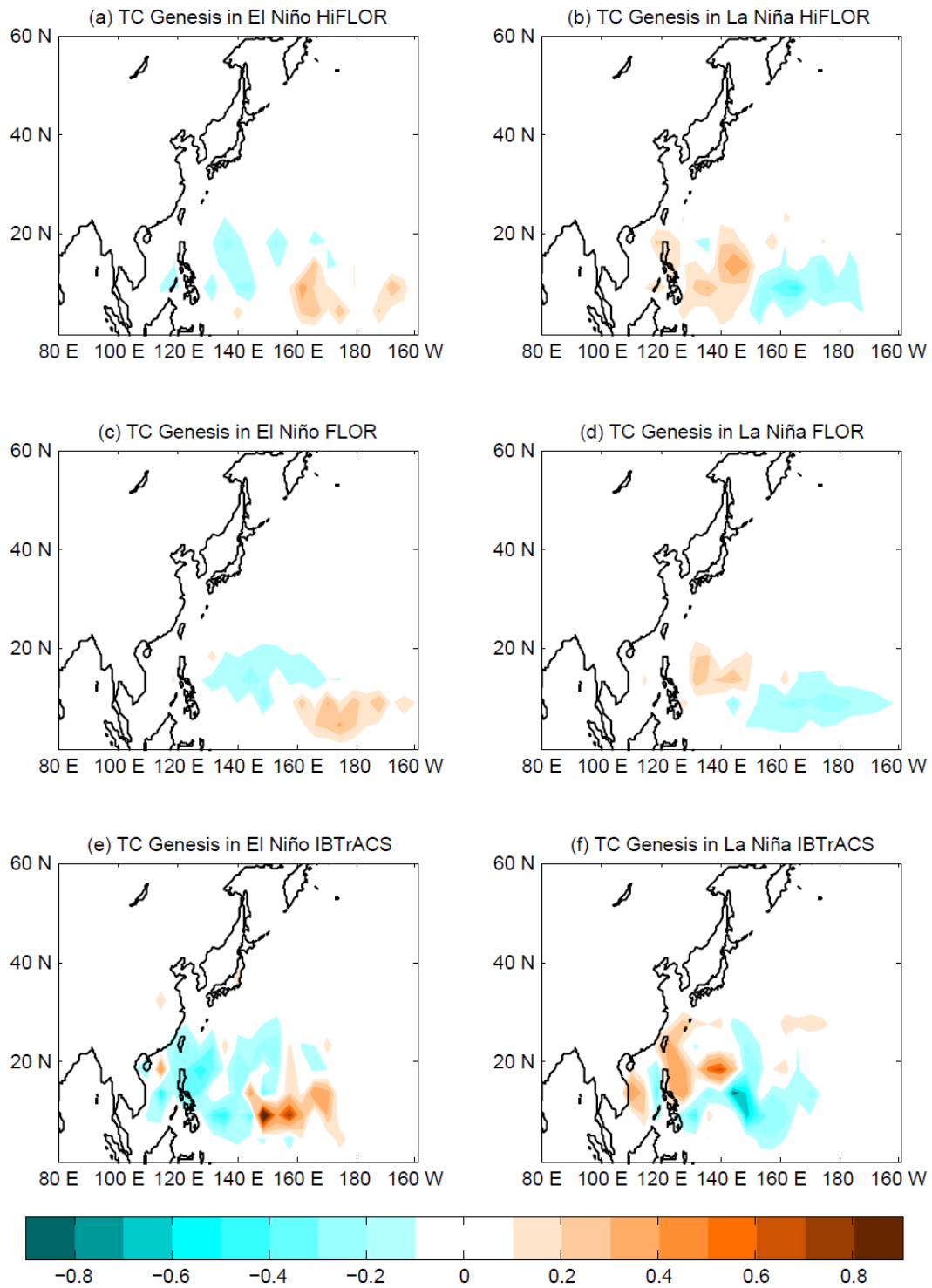
1029
 1030
 1031
 1032
 1033

Figure 12. The simulated TC genesis (unit: times/year) climatology in the SSS- and SST-nudging experiments of HiFLOR, FLOR and observations (1971-2012). The red plus sign represents the mean TC genesis location.



1034

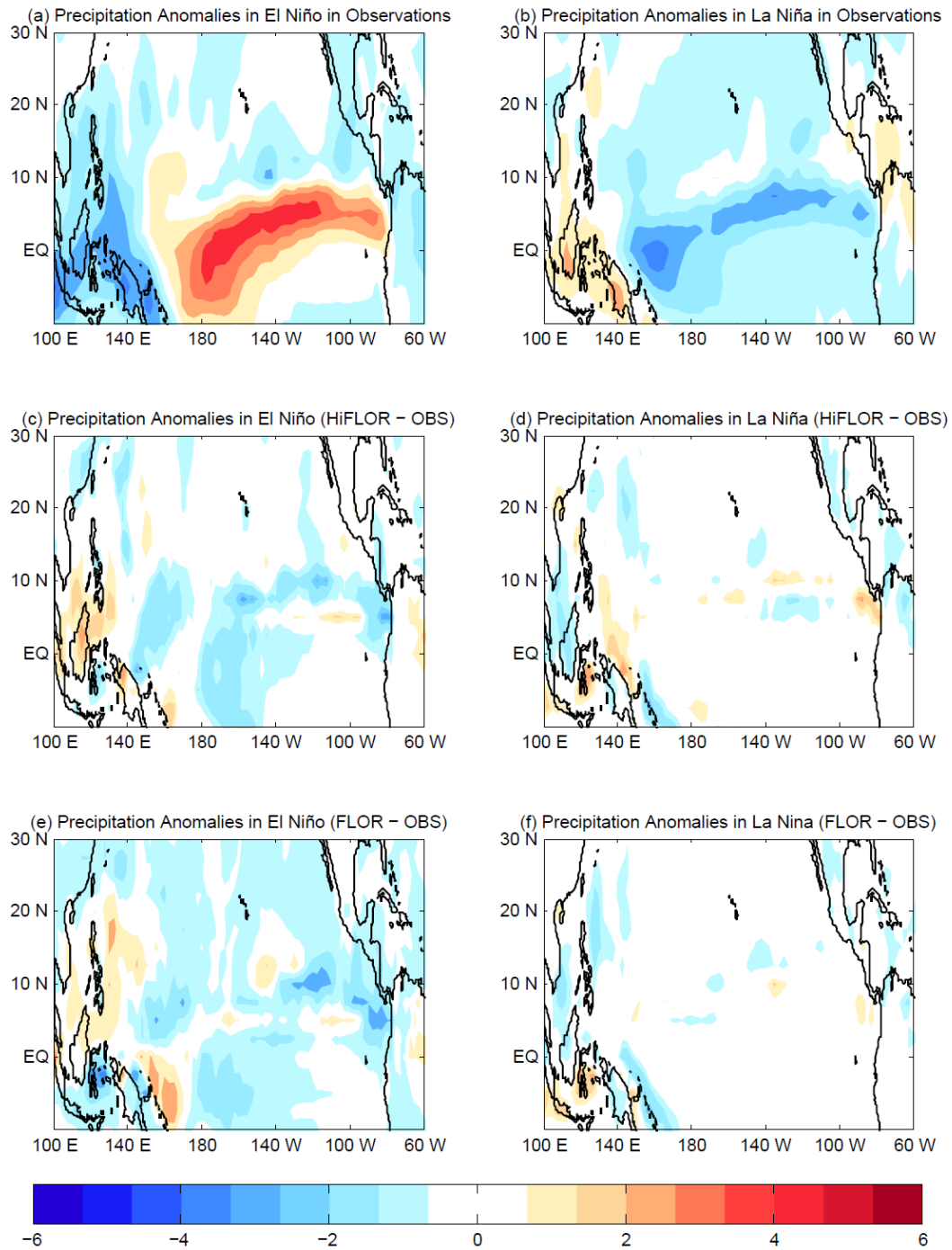
1035 Figure 13. TC track density anomalies (units: times/year; binned into $5^\circ \times 5^\circ$ grid box)
 1036 in El Niño and La Niña events in the SST-restoring experiments of HiFLOR and
 1037 FLOR and the observations.



1038

1039 Figure 14. Annual average TC genesis anomalies (units: times/year; binned into $5^\circ \times 5^\circ$
 1040 grid box) during El Niño and La Niña events in SST-restoring experiments with
 1041 HiFLOOR, FLOR and observations.

1042



1043

1044 Figure 15. Precipitation anomalies (unit: mm/day) during El Niño and La Niña phases
 1045 based on observations (a,b), SST-restoring HiFLOr-observations (c,d) and
 1046 SST-restoring FLOR-observations (e, f).

1047

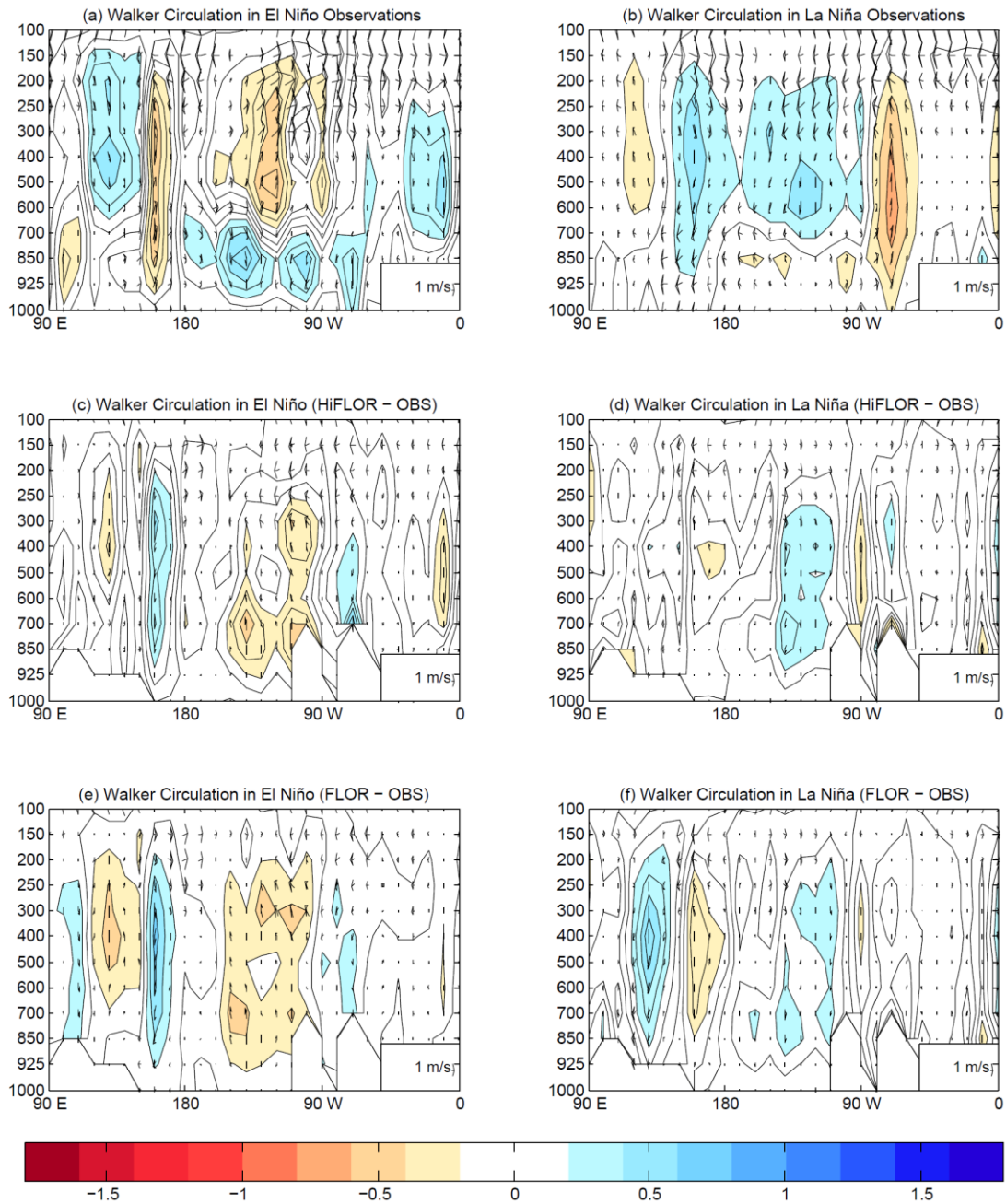
1048

1049

1050

1051

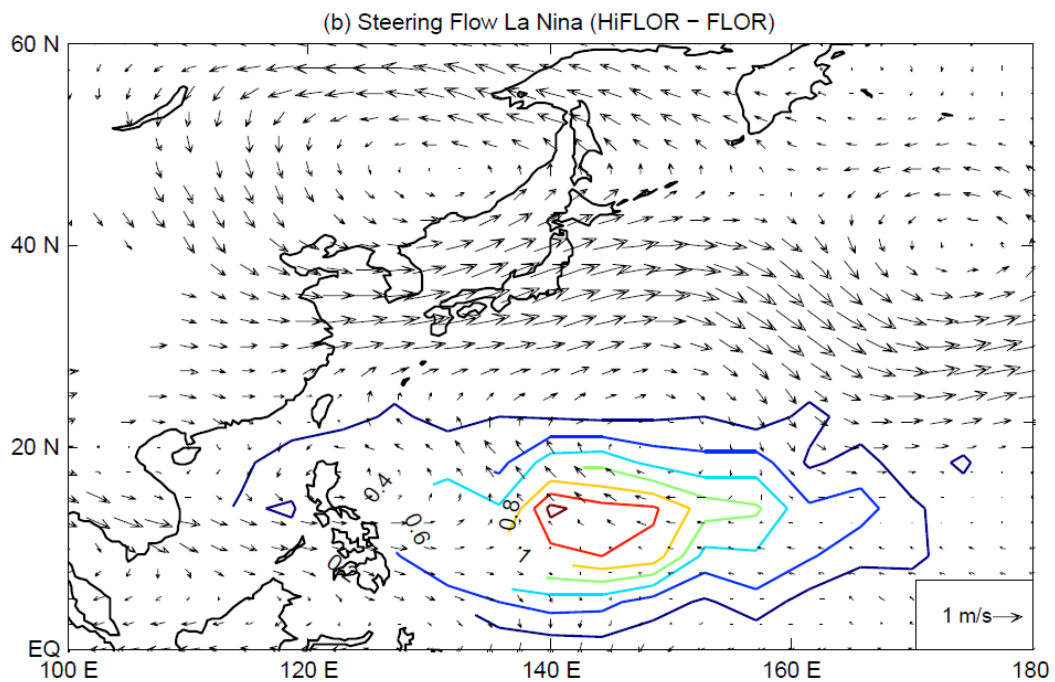
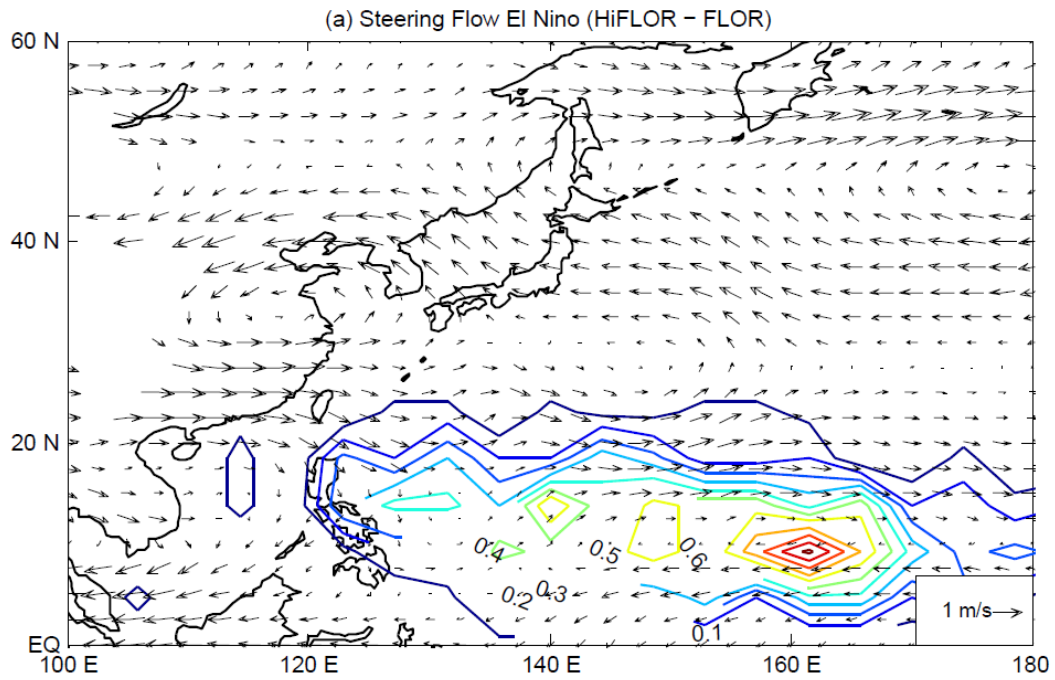
1052



1053

1054 Figure 16. Vertical profile of wind vector [zonal wind (averaged over 5°N to 20°N)
 1055 and $-50 \cdot \omega$ (unit: pa/s)] during El Niño and La Niña phases based on observations
 1056 (a,b), SST-restoring HiFLOr-observations (c,d) and SST-restoring
 1057 FLOr-observations (e, f) to depict the Walker circulation. "OBS" represents
 1058 observations. The shading in this figure represents ω (omega).

1059



1060

1061 Figure 17. Steering flow (unit: ms^{-1}) (HiFLOr minus FLOR) in the SST-restoring
 1062 experiments during the El Niño (a) and La Niña (b) phase. Contours represent the
 1063 annual average TC genesis density in HiFLOr.

1064